Combustion and Flame 280 (2025) 114355

Contents lists available at ScienceDirect

Combustion and Flame

journal homepage: www.sciencedirect.com/journal/combustion-and-flame

Automatic generation of compact kinetic models for large alkane oxidation

Sirio Brunialti [a,*], Xiaoyuan Zhang [b], Qi Wang [a], Tiziano Faravelli [c], S. Mani Sarathy [a]

[a] Clean Energy Research Platform, Physical Sciences and Engineering (PSE) Division, King Abdullah University of Science and Technology, Thuwal 23955-6900, Saudi Arabia
[b] Department of Thermal Science and Energy Engineering, University of Science and Technology of China, Hefei 230026, Anhui, China
[c] Department of Chemistry, Materials, and Chemical Engineering, Politecnico di Milano P.zza Leonardo da Vinci 32, 20133 Milano, Italy

ARTICLE INFO

Keywords:
Alkanes
Kinetics
Oxidation
Automatic
Fuel
Low temperature
E-fuel

ABSTRACT

Large alkanes are principal chemical components in many petroleum and alternative renewable fuels. The development of oxidation models for large alkanes is often complex and time-consuming. A methodology for the automatic generation of detailed and lumped kinetic models of oxidation of large alkanes is presented herein. This procedure is built upon the authors' previous work (Brunialti et al., 2023), wherein an automatic procedure for generating oxidation models of alkanes based on MAMOX++ software was developed. The procedure is based on a rate rule approach, and it can generate detailed and lumped reaction mechanisms. A new set of rate rules was developed to better describe the reactivity of large alkanes at high and low temperatures. The procedure also includes automatic thermochemical-property computation. The reaction mechanism generation procedure was reviewed to minimize the reaction mechanism size and required user inputs. Detailed reaction mechanism and lumped reaction mechanisms were generated for 40 alkanes with a carbon number of 5–16. The model predictions were compared with experimental data obtained from jet-stirred reactors, shock tubes, rapid compression machines, and laminar burning velocities. Validations were performed for 30 alkanes under a broad range of temperatures, pressures, and equivalence ratios. The predicted and measured values exhibited good agreement under all conditions for all fuels except for large, highly branched alkanes. The lumped models can reproduce the predictions of the detailed models with high fidelity under all explored conditions while considerably reducing the number of species and reactions involved in the reaction mechanism. Software capabilities for modeling the reactivity of extremely large alkanes were assessed in a comparative study for linear alkanes with up to 30 carbon atoms. Detailed and lumped models for gasoline primary reference fuel mixtures were generated and validated to demonstrate the procedure capabilities for generating compact, task-tailored models.

Novelty and Significance Statement

The novelty of this work lies in the newly developed set of rate rules for the oxidation of large alkanes combined with an updated automatic lumped model generation. The proposed methodology allows for the rapid generation of compact oxidation reaction models for surrogate species representative of diesel, kerosene, and jet fuels. Thus, this work makes it possible to perform accurate numerical simulations of combustion units with any arbitrary mixture of alkanes. Applications of this methodology may range from the design and performance assessment of e-fuels to engine optimization and design.

1. Introduction

The primary goals of energy transition are to increase energy efficiency while gradually phasing out non-renewable fuel use. Nevertheless, hydrocarbon combustion is expected to be important even in the distant future [1]. Biofuels and liquid hydrocarbon e-fuels are carbon-neutral energy vectors that exhibit many desirable features of liquid petroleum fuels, such as high energy density, storage affordability, and simple compatibility with current energy infrastructures [2]. Owing to these properties, liquid hydrocarbon fuels are the only feasible energy alternative for sectors such as aviation. However, research on

* Corresponding author.
E-mail address: sirio.brunialti@kaust.edu.sa (S. Brunialti).

https://doi.org/10.1016/j.combustflame.2025.114355
Received 19 January 2025; Received in revised form 14 July 2025; Accepted 15 July 2025
Available online 19 July 2025
0010-2180/© 2025 The Combustion Institute. Published by Elsevier Inc. All rights are reserved, including those for text and data mining, AI training, and similar technologies.

new liquid fuels and their applications is often hindered by the lack of kinetic models describing their oxidation.

Automatic kinetic model generation is a powerful tool that can provide kinetic models for numerous arbitrarily defined fuels. We define a "reaction mechanism" as a set of reactions and associated kinetic parameters for a specified system, and a "kinetic model" as a reaction mechanism together with thermodynamic and transport data needed for simulating reacting flows. Over the years, several automatic reaction mechanism and kinetic model generation codes, such as the Reaction Mechanism Generator, EXGAS, and MAMOX++, have been developed [3–5]. The available solutions differ in terms of model performance, range of fuels covered, code execution time, required user-provided inputs, and reaction mechanism size. An effective tool for the exploration and performance assessment of new liquid fuels should tackle all the problems involved in the task. First, reduced computational times are highly preferable, since fuel design may involve the generation of several reaction mechanisms for a set of candidate fuels. Moreover, real fuels are often blends of many pure components. Second, acceptable model performances must be achieved for large hydrocarbon species with carbon numbers of up to 16–20, in order to describe the gas-phase reactivity of many real fuels. Thurs, the model size must be limited. Kinetic models for large species may involve thousands of species and tens of thousands of reactions [6,7], thereby making the model unsuitable for the complex simulations required for describing real combustion systems.

MAMOX++ was originally developed by Ranzi et al. [5,8] for the automatic generation of detailed and lumped reaction mechanisms for the oxidation of noncyclic alkanes. The code generates kinetic sub-mechanisms of oxidation for alkanes whose structures are provided by the user. First, a detailed reaction mechanism is generated using a rate rule-based approach; then, the detailed reaction mechanism is used as a reference for generating a lumped mechanism. Since the generated reaction mechanisms define both forward and reverse reaction rate constants for reversible reactions, they are only marginally affected by the thermochemical properties of the species, making MAMOX++ *a* valuable candidate for exploring the reactivity of large alkanes. Recently, the authors developed a new procedure based on MAMOX++ software; this procedure results in a better representation of low-temperature oxidation and generates accurate and predictive lumped reaction mechanisms [9]. New reaction classes were added to simulate the reaction pathways relevant to low-temperature oxidation. Moreover, a new set of rate rules was compiled using the latest state-of-the-art measurements from the literature. A new lumping procedure was designed, and this procedure yielded an accurate representation of the combustion process under all the combustion-relevant conditions. Thus, the previously proposed methodology of the authors could describe the reactivity of linear and branched alkanes with up to 10 carbon atoms. Both low- and high-temperature reactivity values were predicted accurately by the compact lumped mechanism generated by the software. However, the mechanisms generated with the former procedure [9] for alkanes with >11 carbon atoms yielded unsatisfactory performance. There were considerable discrepancies between the predictions of the detailed model and experimental measurements at high and low temperatures, with the performance decreasing with an increase in alkane size [9].

The present work expands automatic reaction mechanism generation functionalities to improve large alkanes modeling accuracy. An updated set of rate rules is developed. Detailed reaction mechanism generation and the lumping procedure are improved. The applied modifications are tested by generating detailed and lumped models for 40 linear and branched alkanes in the range of C_5–C_{16}. The predictions of the model are then compared with a large set of experimental data, covering 30 alkanes. Experimental data from studies on rapid compression machines, shock tubes, jet-stirred reactors, and laminar flame burners are presented for model validation. The data covers a wide range of temperatures, pressures, and mixture compositions. The lumping procedure is also examined to demonstrate the robustness and accuracy of the proposed methodology.

2. Methodology

2.1. Detailed mechanism generation

The automatic detailed reaction mechanism generation procedure in MAMOX++ was updated to improve the generation of reaction mechanisms for large alkanes. MAMOX++ generates the oxidation submechanism of the target alkane by compiling the set of possible reactions belonging to a predefined set of reaction classes. The list of considered reaction classes in the previous work of the authors [9] is given in Table 1. To limit reaction mechanism size, some reaction pathways and species classes relevant to certain combustion environments were omitted. This work focuses on alkane oxidation chemistry of relevance to combustors, so pathways under pyrolysis or low-temperature oxidation leading to hydrocarbon molecular growth (e.g., polycyclic aromatic hydrocarbons in soot pathways, oxidative deposit formation) were neglected. In the case of mixtures, cross reactions between fuel radicals were neglected despite their importance under some conditions where deposit formation is important, i.e., fuel filters, injectors, engine liners, etc. [10]. Pathways leading to formation of noncyclic ethers were neglected owing to their minor influence on overall reactivity; this simplification was commonly adopted in prior alkane oxidation models [6,7,11,12]. Moreover, reaction classes involving the third oxygen addition [13–16] and subsequent decomposition reactions, pathways leading to the formation of carboxylic acids, and reactions producing diones were neglected, due to their limited impact of broad combustion phenomenon [17–19]. Intermediate species such as cyclic ethers with alkyl radical side chains and species containing both carbonyl and alkyl radical functionalities were substituted

Table 1
Considered reaction classes. The reaction classes added to the list in the authors' previous work are in bold [9].

#	Reaction class	Rate rules reference
1	Unimolecular fuel decomposition	[5,7,24,25]
2	H-abstraction from fuel	[5,7,11,24]
3	Alkyl radical isomerization	[5]
4	Alkyl radical beta decomposition	[5]
5	Alkyl radical decomposition to alkenes from O_2 addition	[5]
6	O_2 addition to alkyl radical	[26]
−6	O_2 removal from alkyl peroxy radical	[5]
7	Alkyl peroxy radical isomerization	[11,20,27]
−7	QOOH isomerization	[28]
8	O_2 addition to QOOH	[11]
−8	O_2 removal from OOQOOH	[5]
9	Conversion of OOQOOH to ketohydroperoxide	[11,27]
10	Ketohydroperoxide decomposition	[11,21]
11	HO_2 concerted elimination from alkyl peroxy radical	[11,28]
12	Cyclic ethers formation	[11,20,28]
13	QOOH decomposition	[11,28]
14	OOQOOH isomerization to $P(OOH)_2$	[11,27]
−14	$P(OOH)_2$ isomerization to OOQOOH	[28]
15	HO_2 concerted elimination from OOQOOH	[11,28]
16	Cyclic ether-OOH formation from $P(OOH)_2$	[11,28]
17	$P(OOH)_2$ decomposition	[11,28]
18	Alkenyl-OOH decomposition	[11,21]
19	Cyclic ether-OOH decomposition	[11,21]
20	Cyclic ethers decomposition	[11]
21	H-abstraction from alkenes	[11]
22	Alkenyl RO formation	[11]
23	Alkenyl RO decomposition	[11,29]
24	**Aldehydes and ketones decomposition**	[5,7,11,24,25]
25	**Unimolecular decomposition of alkene**	[11]
26	**Alkenyl radical beta decomposition**	[11]
27	**Hydrogen addition to alkene**	[11]
28	**Enones and enals decomposition**	[5,7,24,25]

with their decomposition products following alkyl radical β-scission pathways. Dienes, formed by the β-scission of allylic radicals, were replaced with their decomposition products obtained by homolytic cleavage of the single bond connecting the two olefinic groups.

The list of species classes in the alkane sub-mechanisms is given in Table 2. Notably, automatic generation decomposition reactions for large aldehydes, ketones, enones, and enals were added to MAMOX++. The automatic generation of such reactions is not critical for small alkanes (the ones that could be predicted well by the previous version of MAMOX++) because most of these reactions are already included in the core/base C1-C4 reaction mechanism. However, the decomposition of oxygenated intermediates from large alkanes (C_{11} and above) is missing in the base mechanism. Therefore, the presented rate rules included new reaction classes for the decomposition of aldehydes and ketones (class 24) and enones and enals (class 28). The decomposition reactions occur through hydrogen abstraction by the OH radical and subsequent alkyl radical beta decomposition; when this pathway is not possible, homolytic cleavage of carbon–carbon bonds occurs instead. Moreover, high-temperature decomposition pathways for alkenes (i.e., olefins) and allylic radicals were added. Specifically, unimolecular decomposition of alkenes (class 25), alkenyl radicals β-scission (class 26), and hydrogen addition to alkenes (class 27) were included. These high-temperature pathways are crucial for describing the decomposition of alkenes and allylic radicals in flames, where bimolecular reactions with hydroxyl radical (class 21), and hydroperoxyl radical (class 22) are less important due to low oxygenated radical concentrations.

The original MAMOX++ procedure allowed for the generation of separate sub-mechanisms for each of the user-defined target alkane. Merging the sub-mechanisms and the integration of the core mechanisms was left to the user. This raises a major challenge for the compilation of large alkane mechanisms. Indeed, the decomposition of large alkanes leads to the formation of species belonging to the sub-mechanism of smaller alkanes. To include the reactive pathways of such smaller species, the complete sub-mechanism of their parent alkane must be generated. This solution is not practical when large species are involved as numerous species are generated in the decomposition reactions. The previous methodology, therefore, led either to excessively large mechanisms (when all the complete sub-mechanisms of the required alkane are included) or to incomplete mechanisms. Therefore, the detailed mechanism generation procedure was altered in this work.

The updated methodology requires the user to define the list of alkanes for which the complete oxidation mechanisms are desired. The software generates the full kinetic sub-mechanism only for these specified alkanes and merges the sub-mechanisms, integrating the user-provided core/base mechanism. Finally, the software identifies all the intermediate species without a consumption pathway and generates their consumption reactions, without requiring the full sub-mechanism of their parent alkanes. This approach leads to the smallest complete reaction mechanism capable of representing the oxidation of the user-defined fuels.

Table 2
Species classes.

Short name	Species class
HC	Fuel
R	Alkyl radical
ROO	Alkyl peroxy radical
QOOH	QOOH species
OOQOOH	OOQOOH species
$P(OOH)_2$	$P(OOH)_2$ species
OLE	Alkene (olefin)
cEth	Cyclic ether
cEth-OOH	Cyclic ether-OOH
OLE-OOH	Alkene-OOH (olefin-OOH)
KHP	Ketohydroperoxide
OLE-R	Alkenyl radical
alkRO	Alkenyl RO species
ALK/KETO	Aldehyde/ketone
OLE-CO	Enal/enone

For some specific reaction pathways, the rate rules were not available in the reference studies. Therefore, the missing rules were obtained by modifying the rate rules of similar reaction pathways. The rate rules proposed by Zhang et al. [11] for the isomerization of ROO (class 7) species do not include values for some of the reactive pathways involving secondary and tertiary carbons. These rate rules are relevant for describing the reactivity of large, branched alkanes. The effect of the substitution degree of the reactive carbons was considered by applying the corrections proposed by Miyoshi [20] to the rate rules proposed by Zhang et al. [11]. Similarly, the effect of embedded substituted carbons on the formation rate of cyclic ethers from QOOH species (class 12) was considered. The rate rules for the formation of cyclic ethers proposed by Zhang et al. [11] were modified according to the corrections proposed by Miyoshi [20]. The detailed reaction classes, the rate rules, and methods adopted for the generation of the products of the reactions are provided in the Supplementary Materials. The proposed rate rules were input to the software to define kinetic parameters of each reaction in the detailed reaction mechanism. No tuning or modification of individual kinetic parameters was performed.

The detailed reaction mechanisms obtained by the proposed automatic methodology are comparable in structure, number of species, classes of species, number of reactions, and classes of reactions to widely adopted alkane combustion models [7,11,12,21–23].

2.2. Lumped mechanism generation

The software also generates a separate and distinct lumped reaction mechanism from the detailed reaction mechanism. Lumping is defined as the grouping of isomers (i.e., horizontal lumping) into a single species, thereby reducing the total number of species in the reaction mechanism. This reduction technique relies on the similar reactivity of isomers. Therefore, it is assumed that grouping similar isomers does not lead to relevant variations in model predictions. Furthermore, grouping isomers also allows grouping of their respective reactions. Thus, lumping reduces the number of species, and the number of reactions involved in the reaction mechanism. The efficacy of this lumping methodology in kinetic modeling of combustion processes has been extensively proven [30–34].

It is noteworthy that generally, lumped reactions are not elementary reactions. Even when a lumped reaction is defined to represent a group of elementary reactions, the definition of the transition state in the lumped reaction may be ambiguous. Therefore, it cannot be assumed that the kinetics of lumped reactions strictly respect the thermodynamic consistency. For this reason, defining the kinetics of both forward and backward reactions for reversible reactions is crucial.

The procedure adopted for generating lumped mechanisms is based on our previous work [9]. Each fuel's detailed sub-mechanism is used as a reference for generating the corresponding lumped sub-mechanism. A single lumped reaction is defined for each reaction class in the detailed sub-mechanism. Similarly, a single lumped species is defined for each species class of species in the detailed sub-mechanism. Following these criteria, the reactions and species for the lumped sub-mechanism are compiled. The rates and stoichiometric coefficients of the lumped reactions are computed by fitting predicted species' rates of consumption and production obtained using the detailed model in homogeneous combustion simulations. Further details on the computation of lumped mechanisms parameters can be found in the previous work of the authors [9], and briefly summarized here.

The kinetic parameters in the lumped reaction mechanism are functions of simulated species distributions. Kinetic parameters were chosen by minimizing an objective function that calculates the difference in predicted species distributions between the lumped and detailed models. The differences are quantified by the ratio of concentration of any given lumped species X_i over the sum of concentrations of all species

X represented by the corresponding lumped species.

In our previous work [9], homogeneous continuous stirred-tank reactor (CSTR) simulations were adopted to retrieve the species concentration predictions according to the detailed mechanism. The isomer distributions in CSTR simulations appeared to be strongly affected by temperature and pressure only. This phenomenon can be observed in Fig. 1, where the distribution of the alkyl peroxide isomers derived from isooctane oxidation in CSTR is displayed. Notably, a negligible effect of equivalence ratio and residence time is observed on the isomer distributions. Therefore, the rate of the lumped reactions, that is defined as a function of the isomer distributions, was represented as a function of temperature and pressure only. For this reason, the reference simulations were performed at different temperatures and pressures, computing the isomer distributions for each condition. Subsequently, according to the lumping procedure, the rate of the lumped reaction was computed at each temperature and pressure, and its value was represented with a PLOG formulation of the reaction rate.

In this work, constant-volume homogeneous batch reactor simulations were also utilized to retrieve species concentrations. In batch reactor simulations, the concentrations were considered as the time average concentration from the beginning of the simulation to mixture ignition, which is marked by the peak of OH radical concentration. In this way, two lumped mechanisms were generated—one based on CSTR predictions and the other based on constant-volume homogenous batch reactor predictions. The performances of the two mechanisms in replicating the predictions of the detailed mechanism were compared. Both CSTR and batch simulations were performed with stoichiometric mixtures of fuel in air. For CSTR simulations, the residence time was set as 2 s. The arbitrary choice of the equivalence ratio and residence time was supported by the low influence of these parameters on the distributions of the isomers, as already discussed above.

In CSTR simulations, isomer distributions can be computed using solely the oxidation sub-mechanism of the parent alkane, while for batch simulations, the core/base reaction mechanism is needed to represent OH radical formation up to ignition. Simulations were performed at different temperatures and pressures of 600–1200 K and 1–64 atm,

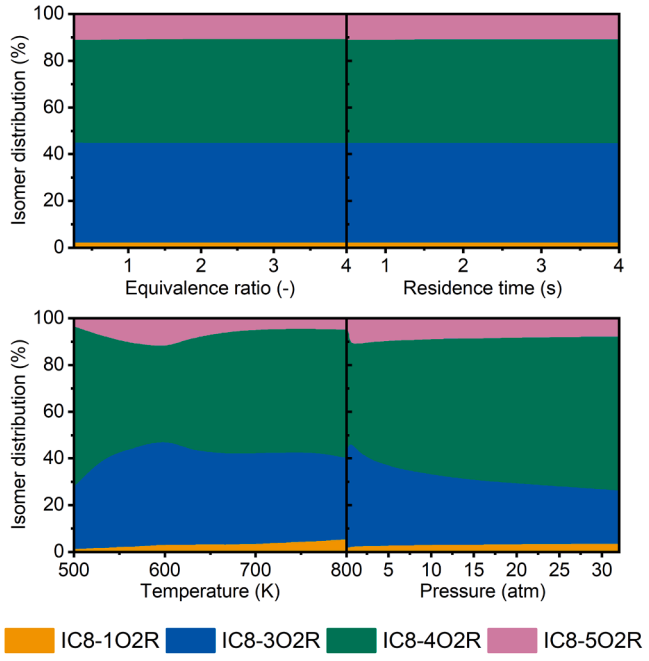

Fig. 1. Distributions of the alkyl peroxides of isooctane as predicted by the CSTR simulations based on the detailed mechanism. Simulation parameters (unless the subject of a parametric analysis) are isooctane/air, 570 K, 1 atm, a residence time of 2 s, and an equivalence ratio of 1.

respectively. Simulations were performed in MAMOX++ using the *C++* interface of Cantera 3.0 toolkit [35], and parameters were fitted using the NLopt library for *C++* [36]. The workflow of the generation and validation of the models is represented in Fig. 2.

2.3. Thermochemical data generation

As discussed in Section 1, the kinetic model is only slightly influenced by species' thermochemical properties because both forward and reverse rate constants are defined independently; hence, reverse rate constants are not computed based on the principle of microscopic reversibility. However, thermochemical properties are needed to solve the energy equation during reactor simulations. MAMOX++ software was updated to add thermochemical property estimation. For all species included in user-provided core reaction mechanism, the thermochemical properties in the core kinetic model are adopted. For newly generated species, an automatic Benson's group additivity methodology [37] was implemented. Although group additivity methods rarely provide predictions accurate enough to describe the kinetics for large species, they are sufficiently accurate to describe the heat release.

The thermochemical properties of the lumped species are computed considering each lumped species as a mixture of its representative isomers. Temperature-dependent thermochemical properties and distributions of the individual isomers are known from CSTR and batch reactor simulations, the thermochemical properties of the lumped species can be computed by adopting ideal gas mixing rules.

$$\Delta H_X^f(T) = \sum_{i=1}^{NI} \delta_i(T) \Delta H_{X_i}^f(T). \quad (1)$$

Eq. (1) can be used to compute the temperature-dependent heat of formation of a lumped species *X*, where $\Delta H_X^f(T)$ is the temperature-dependent heat of formation of a generic lumped species *X*, *NI* is the number of different isomers represented by the lumped species *X*, δ_i is the temperature-dependent distribution of the *i th* isomer represented by the lumped species *X*, and $\Delta H_{X_i}^f(T)$ is the temperature-dependent heat of formation of the *i th* isomers represented by the lumped species. Computing the lumped species thermochemical properties was based on the distribution of the isomers at atmospheric pressure.

The software including all the upgrades described in this section is available at https://github.com/BSirio/Mamox_2.

2.4. Transport data and mechanism reduction

Transport properties of the species in the detailed model were computed via the automatic property estimator implemented in the Reaction Workbench toolkit of Chemkin PRO. For lumped species, the transport properties of an arbitrarily chosen isomer were adopted. This choice is justified by the small differences between the transport properties of the isomers. For flame simulations, detailed kinetic models were automatically reduced by removing low-temperature chemistry with the high-temperature sub-mechanisms extraction tool provided in Reaction Workbench. Similarly, the lumped models were manually reduced by removing the low-temperature sub-mechanisms. Both mechanism reduction methods removed reactions and species belonging to reaction classes 6 to 20 (see Table 1). Moreover, for the simulations concerning *n*-dodecane, all the sub-mechanisms of branched alkanes and the sub-mechanisms of linear alkanes with >12 carbon atoms were removed. These reduced mechanisms are provided in the Supplementary Materials.

2.5. Simulations for model validation

Chemkin PRO [38], Zero-RK zero-dimensional solvers [39], OpenSMOKE++ framework [40], and Cantera [35] were adopted to perform simulations for model validation. Different software solutions were used

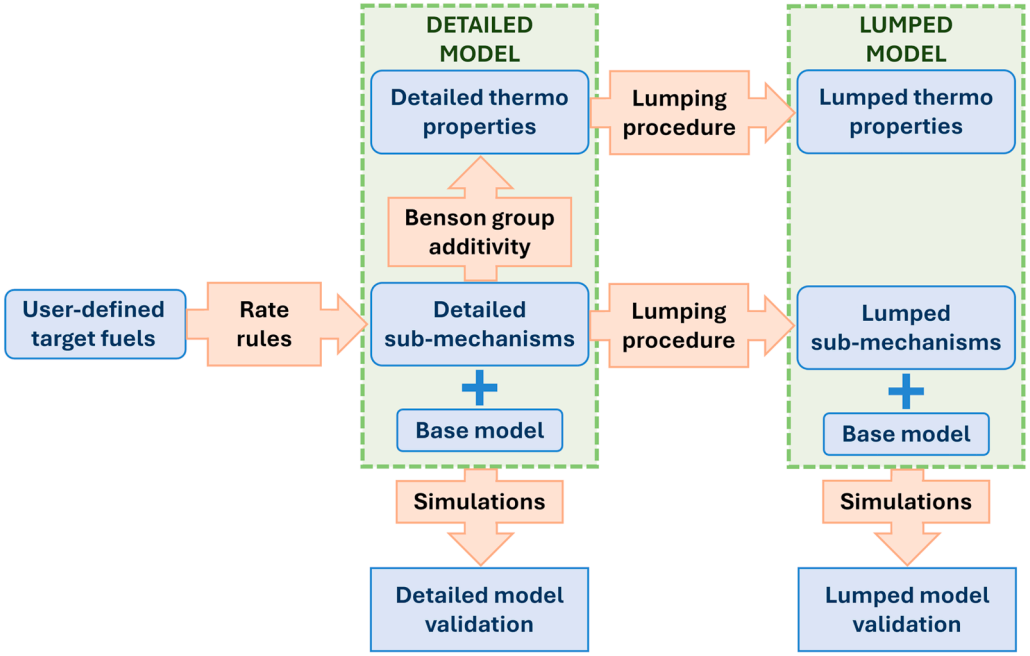

Fig. 2. Mechanism generation and validation workflow.

due to the large number of simulations required. The faster solver for each kind of simulation was chosen. Zero-RK was adopted for the simulation of homogeneous conditions based on the detailed model due to its fast solvers for large models. Several failed simulations were performed in Chemkin PRO, which showed better convergence than Zero-RK for some cases. Chemkin PRO was also adopted to simulate one-dimensional flames based on the detailed model. OpenSMOKE++ was utilized to simulate homogeneous reactor simulations with lumped models due to its ability to efficiently handle stiff kinetics. Indeed, OpenSMOKE++ allows the user to adopt tailored solvers for dense Jacobians that are characteristic of lumped kinetic models. One-dimensional flame simulations based on the lumped models were performed with Cantera, exploiting a script developed by the authors to perform multiple simulations in parallel on a cluster. All the adopted software solutions are well established, and no appreciable differences were observed between the results obtained by different solvers. Flame speed simulations adopted a mixture-averaged transport model. Adaptive grids were adopted for flame simulations, imposing maximum gradient of 0.1 and maximum curvature of 0.5 for detailed model simulations performed with Chemkin PRO, while thresholds of 0.06 for the gradient, and 0.12 for the curvature, were set for lumped model simulations performed with Cantera.

3. Results and discussion

3.1. Model generation

The detailed and lumped models comprising the complete sub-mechanisms of 40 alkanes were generated using the proposed methodology. The list of targeted alkanes comprised the main alkanes studied in combustion kinetics. Notably, linear alkanes from pentane to hexadecane, 2-methyl alkanes from pentane to dodecane, isooctane, and isocetane. Other methyl-substituted alkanes were also included when relevant literature experimental measurements were available. Moreover, some alkanes were included to account for the chemistry of the main moieties generated by the decomposition of larger alkanes. Table 3 shows the 40 selected alkanes alongside the conditions of the experimental measurements used for model validation. Both lumped and detailed sub-mechanisms were merged with the AramcoMech 2.0 core model [41]. The obtained detailed model for 40 alkanes contained 15,024 species and 48,782 reactions, while the lumped model included 1504 species and 5213 reactions. In total, 493 species and 2716 reactions from the core model were included. Hence, the detailed model introduced 14,531 new species and 46,066 new reactions, while the lumped model introduced 1011 new species and 2497 new reactions. The lumped model's reduction in species was achieved by the lumping procedure. Fig. 3 shows the dependency of the reaction mechanism size on alkane size for the detailed and lumped models of linear alkanes. The generated models and the species list are presented in the Supplementary Materials.

The current software implementation of the presented methodology allows for the rapid generation of alkane sub-mechanisms. The detailed sub-mechanisms require generation time in the order of seconds on a modern personal computer, even for larger alkanes. The generation speed of the lumped sub-mechanism is mostly limited by the computational time required for solving all the necessary simulations. As stated in Section 2.2, simulations in the temperature range of 600–1200 K and pressure range of 1–64 atm were investigated. The temperature was discretized into 13 points, while pressure was discretized into 9 points, leading to 91 simulations to generate each lumped sub-mechanism. Using the Cantera 3.0 [35] *C++* interface generates a lumped sub-mechanism in several minutes. Fig. 4 shows the generation time for sub-mechanisms of different linear alkanes, indicating an increase in generation time with the fuel size. Lumped sub-mechanisms based on batch reactor simulations require higher generation times than lumped mechanisms based on CSTR simulations. The higher generation time for the former is due to the inclusion of the core mechanism in the simulation, which considerably increases the computational cost. Despite notable differences in conditions between batch reactor and CSTR simulations, the two cases yield similar isomers' distributions. Fig. 5 shows the temperature-dependent distribution of the alkyl peroxy radicals in isooctane in CSTR and batch simulations.

3.2. Model validation

The automatic mechanism generation procedure was adopted to generate complete detailed and lumped sub-mechanisms for 40 alkanes. This group of alkanes includes both linear and branched species, with

Table 3
List of species whose full oxidation sub-mechanisms are included in the detailed and lumped models, and conditions of the experimental measurements used for model validation. IDT=ignition delay times, JSR=jet-stirred reactor speciation, ST-TH=Shock tube species concentration time histories, LBV=laminar burning velocities.

Species name	Experimental conditions				
	Type	T [K]	P [atm]	Φ [-]	Ref.
n-pentane	-				
n-hexane	JSR	500–800	1.05	1	[42]
	IDT	670–1360	15	1	[11]
n-heptane	JSR	500–1100	1.05	1	[43]
	IDT	660–1280	13.5	0.5–2	[44]
n-octane	JSR	500–1100	1.05	1	[45]
	IDT	650–1260	20	1	[7]
n-nonane	IDT	630–1210	10	1	[46]
n-decane	JSR	550–1100	1	1	[47]
	IDT	690–1300	13.5	0.5–2	[48]
n-undecane	JSR	550–950	10	1	[49]
	IDT	730–1300	11–12	1–2	[50]
n-dodecane	JSR	560–1030	10	1	[49]
	IDT	630–1300	15	0.5–1.5	[51]
	LBV	400–450	1	0.8–1.4	[52]
n-tridecane	-				
n-tetradecane	JSR	560–1030	10	1	[53]
	IDT	880–1300	13–40	0.5–1	[54]
n-pentadecane	IDT	670–1300	10	1–1.5	[55]
n-hexadecane	JSR	550–1050	1	1	[47]
	IDT	670–1800	1.865–7	0.95–1	[56–58]
2-methylbutane	-				
2-methylpentane	JSR	500–825	1.05	1	[42]
	IDT	620–980	15	1	[11]
2-methylhexane	IDT	650–1290	10–40	0.5–1	[59]
	ST-TH	750–828	8	0.089	[60]
2-methylheptane	JSR	530–1160	10	1	[7]
	IDT	630–1330	20	0.5–1.5	[7]
2-methyloctane	IDT	680–1230	10	1	[46]
2-methylnonane	JSR	475–700	1	1	[61]
2-methyldecane	-				
2-methylundecane	-				
3-methylpentanef	JSR	500–825	1.05	1	[42]
	IDT	650–980	15	1	[11]
3-methylhexane	-				
3-methylheptane	JSR	530–1220	10	1	[62]
2,2-dimethylpropane	-				
2,2-dimethylbutane	JSR	550–1075	1.05	1	[42]
	IDT	700–1000	15	1	[11]
2,2-dimethylpentane	-				
2,3-dimethylbutane	JSR	575–1000	1.05	1	[42]
	IDT	670–950	15	1	[11]
2,3-dimethylpentane	-				
2,4-dimethylpentane	-				
2,4-dimethylheptane	IDT	660–1090	10	1	[46]
2,5-dimethylhexane	JSR	560–1150	10	1	[63]
	IDT	700–1250	20	0.5–1	[63]
2,6-dimethylheptane	IDT	630–900	10	0.5–1	[64]
2,7-dimethyloctane	JSR	475–700	1	1	[61]
	IDT	660–1220	15.5	0.5–1	[65]
2,9-dimethyldecane	IDT	620–710	10–20	0.5–1	[66]
3,3-dimethylpentane	ST-TH	718–820	7	0.089	[60]
2,2,3-trimethylbutane	JSR	770–980	1	1	[67]
2,2,4-trimethylpentane	IDT	635–960	20	1	[68]
2,2,4,4-tetramethylpentane	IDT	670–1170	10	1	[46]
2,2,4,6,6-pentamethylheptane	IDT	610–1310	20–40	1–1.5	[69,70]
2,2,4,4,6,8,8-heptamethylnonane	JSR	770–1030	10	1	[71]
	IDT	640–1620	20–40	0.5–1.5	[70,72,73]
	LBV	443–473	1	0.8–1.5	[74,75]

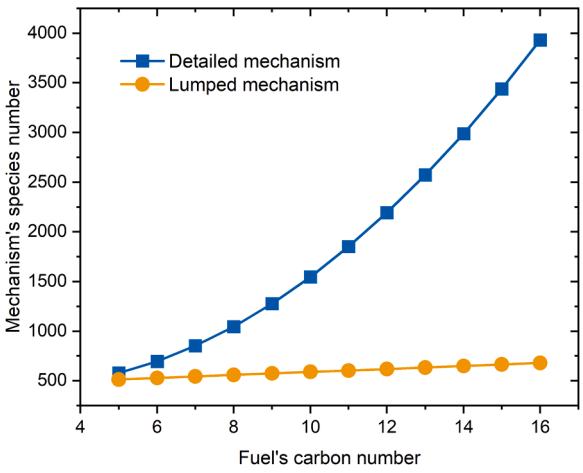

Fig. 3. Sizes of the detailed and lumped models for linear alkanes as a function of the size of the largest included alkane.

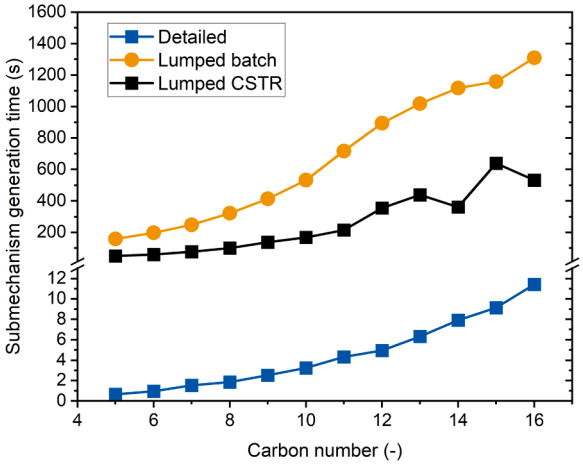

Fig. 4. Generation time for the sub-mechanisms of linear alkanes as a function of alkane size. The generation was performed utilizing four cores of an Intel® Xeon® W-2245 CPU 3.90 GHz.

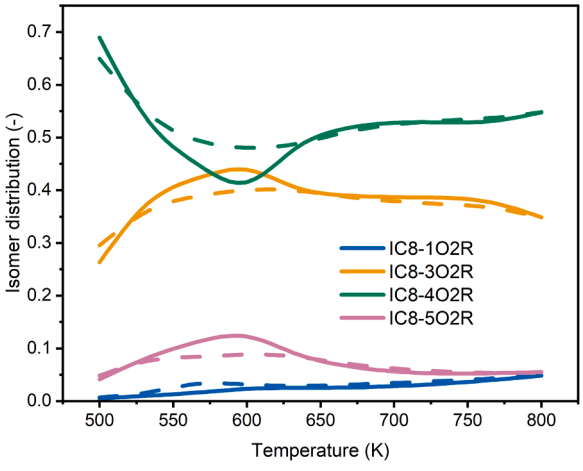

Fig. 5. Alkyl peroxide distribution profiles for isooctane in CSTR (solid lines) and batch reactor (dashed lines) simulations.

5–16 carbon numbers. The generated mechanisms were validated by comparing the predictions of the mechanisms with experimental measurements taken from the literature. The dataset of experimental measurements comprises ignition delay times measurements in rapid compression machines and shock tubes, species concentration measurements in jet-stirred reactors, species concentration time histories in shock tubes, and laminar burning velocities. Data for 30 alkanes, including linear and branched species with carbon numbers of 6–16, were collected and compared. Wide ranges of temperatures, pressures, and equivalence ratios were investigated to test the performance of the models under broad combustion-relevant conditions. Our previous work [9] validated the procedure for alkanes with 10 or fewer carbon atoms. Since little changes were made in the generation of the sub-mechanisms for species with 10 or fewer carbon atoms, validations are only shown for species with 11 or more carbon atoms. A full set of model validations is presented in the Supplementary Materials.

Constant-volume homogeneous adiabatic batch reactor model was used for representing rapid compression machines and shock tubes, while jet-stirred reactors were modeled as homogeneous constant-temperature constant-pressure continuous tank reactors. Laminar burning velocities were computed with the premixed one-dimensional freely propagating flame model. Simulated ignition delay times were defined as the time from the beginning of the simulation to the time at which the maximum temperature gradient of the second-stage ignition occurs. Ignition delay times measurements were scaled to the simulation pressure whenever experimentally measured pressure values were present in the publication. Scaling was performed considering the ignition delay time is proportional to the inverse of the pressure [76]. In the simulations, air refers to a mixture comprising 79 % nitrogen and 21 % oxygen. Stated experimental uncertainties are reported with error bars. More details on experimental uncertainties are available in the Supplementary Material.

Fig. 6 shows the comparison between the predicted and experimental values of ignition delay times for large linear alkanes. The detailed model achieves overall good predictions in replicating the experimental data. The biggest discrepancies appear in the negative-temperature-coefficient (NTC) region; this reflects the high complexity of modeling the kinetics under such conditions. Particularly large discrepancies between predicted and measured ignition delay times can be observed for the oxidation of n-tetradecane at temperatures lower than 1000 K, with the model predicting longer ignition delay times. However, similar deviations can be observed in the modeling works by Westbrook et al. [24] and Mzé-Ahmed et al. [53] as displayed in Fig. 6.

A comparison of predicted and measured species concentrations in the oxidation of linear alkanes in jet-stirred reactors yielded similar results. Fig. 7–10 show the mole fraction profiles of different combustion products and intermediates in the oxidation of large linear alkanes. The values predicted by the detailed model are within the experimental uncertainties for most of the species. When big discrepancies occur, they do not follow a trend applicable to all the investigated fuels, apart from the underprediction of fuel molar fraction at low temperatures. Fig. 11 shows the detailed model performance in the prediction of ignition delay times for branched alkanes. Reactivity is well captured in the high- and low-temperature regimes. However, the model overestimates the reactivity in the NTC regime. Fig. 12 shows a comparison of the predicted and measured species mole fractions during the oxidation of 2,2,4,4,6,8,8-heptamethylnonane (isocetane) in a jet-stirred reactor. Carbon monoxide and water mole fractions are accurately predicted. Model predictions for other combustion products and intermediates were outside the experimental uncertainties at most of the investigated temperatures; nonetheless, the trends of mole fractions and order of magnitudes were overall replicated. These discrepancies indicate that rate rules and thermochemistry need to be revisited for large branched hydrocarbons.

Fig. 6 and Fig. 11 show the ignition delay times predicted by the detailed model; the generated lumped models using CSTR and batch reactor methods are compared for linear and branched alkanes. Small deviations are observed between the detailed and lumped models. Fig. 7–10 and Fig. 12 show the species mole fractions in jet-stirred reactors predicted by the lumped models and compare them with detailed model predictions. The lumped models accurately replicate detailed model predictions for most of the species. The biggest discrepancies

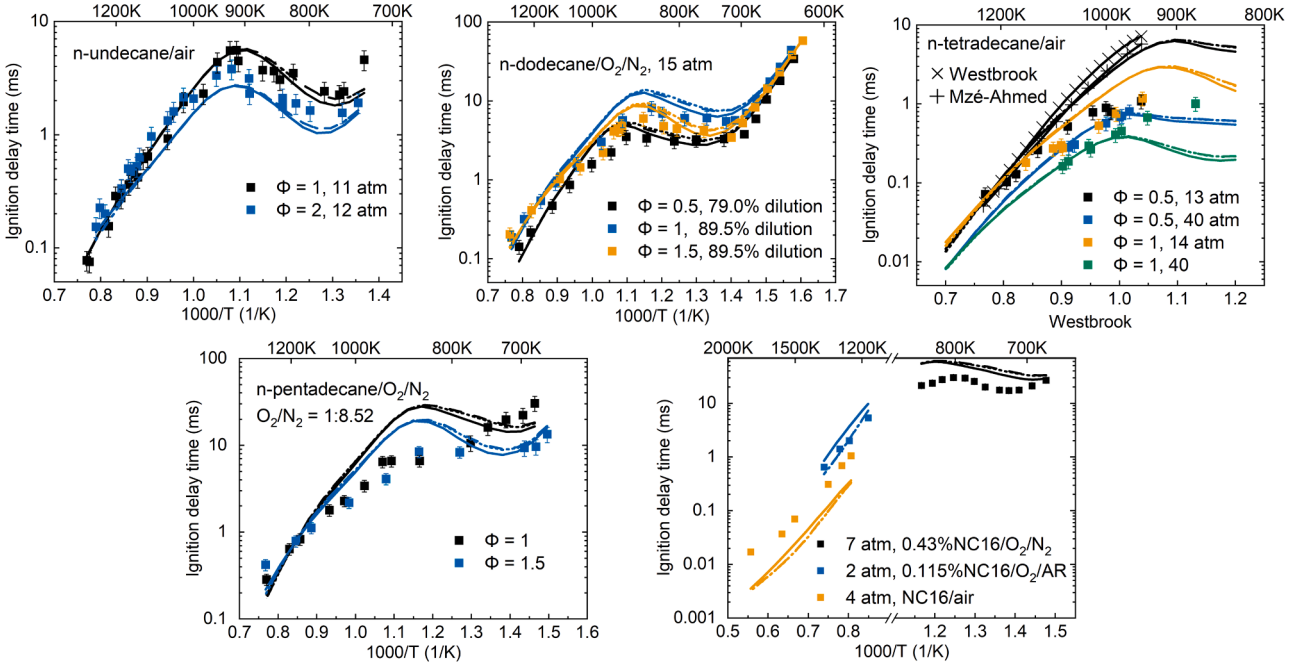

Fig. 6. Simulated (lines and lines plus symbols) and experimental [50,51,54–58] (symbols) ignition delay times of n-undecane, n-dodecane, n-tetradecane, n-pentadecane, and n-hexadecane. Solid lines are detailed model predictions, dashed lines are lumped model predictions based on CSTR simulations, and dotted lines are lumped model predictions based on batch reactor simulations. Lines plus symbols are simulated ignition delay times by two literature models, Westbrook et al. [24] and Mzé-Ahmed et al. [53].

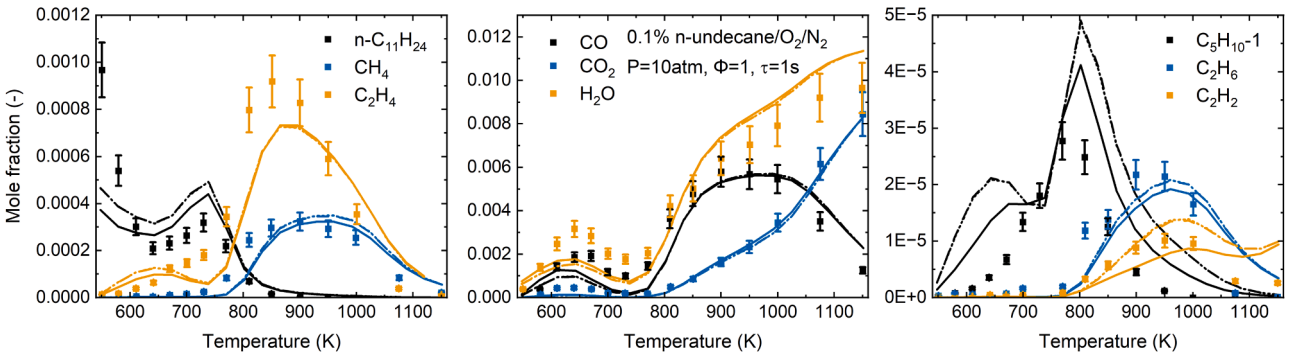

Fig. 7. Simulated (lines) and experimental [49] (symbols) species mole fractions of n-undecane oxidation in a jet-stirred reactor. Solid lines are detailed model predictions, dashed lines are lumped model predictions based on CSTR simulations, and dotted lines are lumped model predictions based on batch reactor simulations.

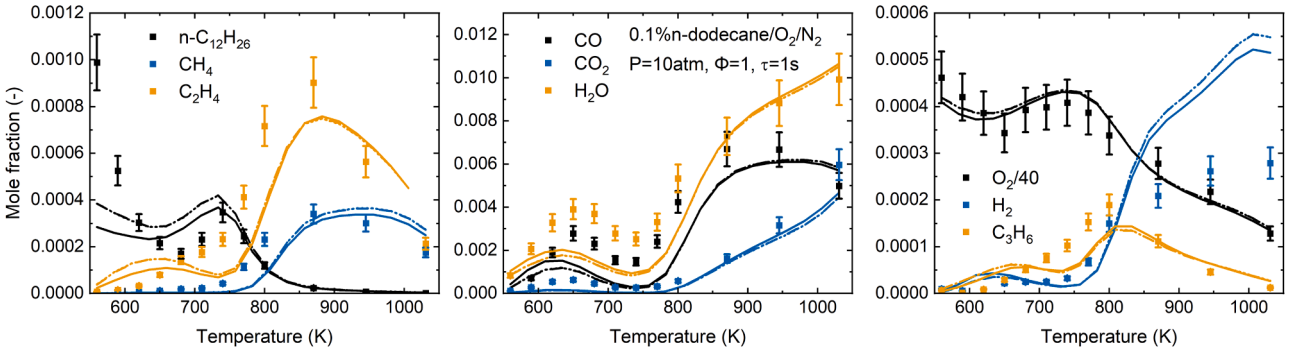

Fig. 8. Simulated (lines) and experimental [49] (symbols) species mole fractions of n-dodecane oxidation in a jet-stirred reactor. Solid lines are detailed model predictions, dashed lines are lumped model predictions based on CSTR simulations, and dotted lines are lumped model predictions based on batch reactor simulations.

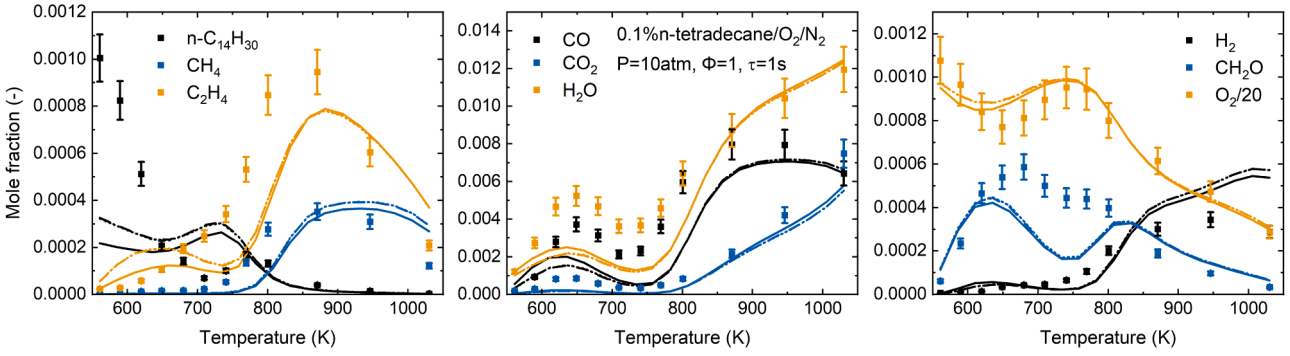

Fig. 9. Simulated (lines) and experimental [53] (symbols) species mole fractions of n-tetradecane oxidation in a jet-stirred reactor. Solid lines are detailed model predictions, dashed lines are lumped model predictions based on CSTR simulations, and dotted lines are lumped model predictions based on batch reactor simulations.

hardly exceed errors of 100 %, and the mole fraction trends and temperature profiles are always reproduced. In all instances, the lumped models provided very similar predictions. The similarity of the two lumped models results from analogous values of isomer distributions (see Section 3.1).

Fig. 13 shows the predicted laminar burning velocities for n-dodecane and isocetane. Predicted laminar burning velocities for n-dodecane fall inside the experimental uncertainty boundaries for most of the tested conditions. Slight overprediction of flame speed can be observed for elevated temperature at stoichiometric conditions. Predictions of the lumped models closely match the predictions of the detailed model. For isocetane, convergence of the detailed models could not be achieved due to the large size of the model, even after the reduction. The lumped models correctly predict flame speeds for fuel-rich conditions. Laminar burning velocities are overpredicted at stoichiometric and fuel-lean conditions, especially at elevated temperatures. This reflects the higher uncertainties for branched species, observed under all conditions. Additional flame speed validations are provided in the Supplementary Material.

The biggest discrepancies between lumped and detailed models can be observed in the prediction of the concentration of intermediate species. The discrepancies are larger for larger alkanes. Such discrepancies mainly arise from differences between the distribution of isomers in the simulated conditions and the reference distribution of isomers adopted in the lumping of the sub-mechanisms of the intermediate species. For this reason, the decomposition of intermediates might be modeled

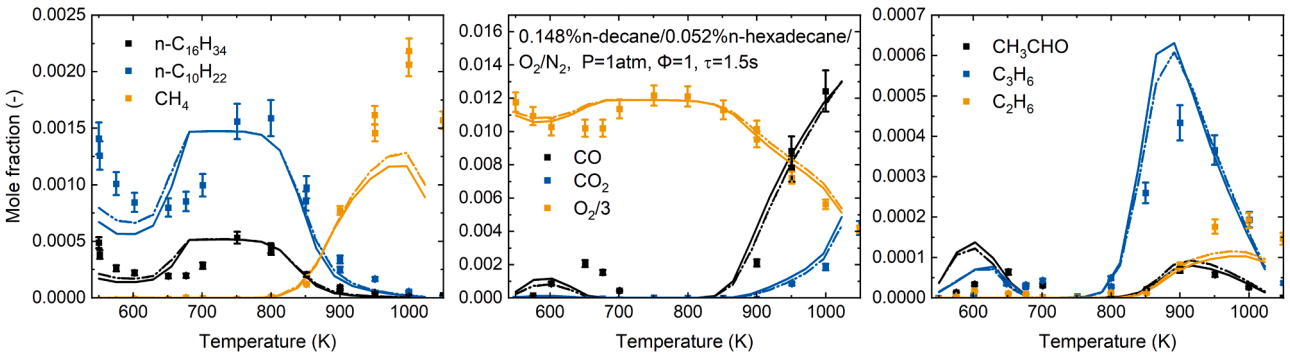

Fig. 10. Simulated (lines) and experimental [47] (symbols) species mole fractions of n-hexadecane oxidation in a jet-stirred reactor. Solid lines are detailed model predictions, dashed lines are lumped model predictions based on CSTR simulations, and dotted lines are lumped model predictions based on batch reactor simulations.

differently in the detailed and lumped models. The main differences stand in the selectivity of the decomposition products between detailed and lumped models. However, while the selectivities can be substantially different when considering the single species, more coherent predictions are observed when considering the selectivities in terms of the produced classes of species. For example, the alkyl radical beta decomposition of an intermediate might lead to the formation of different species in the detailed and in the lumped reaction mechanisms, however, both models will predict the formation of one mole of alkyl radicals and one mole of alkenes for each mole of reacted intermediate. Therefore, the predictions of global combustion properties (e.g., heat generation, ignition delay times, complete combustion products, and laminar burning velocities) are similar between detailed and lumped models.

The ability of the lumped models to accurately represent the detailed models under all the investigated conditions proves the effectiveness of the proposed lumping methodology. In particular, both models perform well in predicting the oxidation behavior under conditions that are different from the simulation conditions under which the isomer distributions were retrieved. This result shows that the lumped models are predictive.

3.3. Sensitivity and error analysis

Model validations showed significant discrepancies between simulated and measured combustion properties for large branched alkanes. This is due to uncertainty in kinetic parameters or a lack of specific rate rules for highly branched molecules. For the sake of directing future research in the identification of accurate rate rules, it is interesting to identify which are the reaction classes that could be the cause of the observed discrepancies. To this end, a sensitivity analysis on ignition delay times was performed. The sensitivity analysis adopted the lumped kinetic model based on CSTR simulations. The use of the lumped model greatly reduces the computational cost of the sensitivity analysis and focuses the analysis on reaction classes instead of single reactions. Indeed, a single reaction in the lumped model represents all the reactions belonging to the same reaction class in the detailed model. The sensitivity parameter of each reaction in the sub-mechanism of the fuel was computed at different temperatures. Each sensitivity parameter was computed by doubling the pre-exponential factor of the corresponding reaction and recording the effect of such change on the simulated ignition delay time. Eq. (2) defines the computed sensitivity coefficient.

$$s_i(T) = (IDT_i(T) - IDT(T))/IDT(T) \quad (2)$$

Where s_i is the sensitivity of the *i th* reaction on the ignition delay time, IDT_i is the simulated ignition delay time when the pre-exponential factor of the *i th* reaction is doubled, and *IDT* is the simulated ignition delay time with the unmodified mechanism.

Sensitivity coefficients are a good metric for identifying which reactions need the highest accuracy in the definition of the reaction rates. The set of important reactions can be further narrowed down by focusing on the region of conditions where the model performs the worst. For this sake, a deviation factor was defined as the relative difference between the experimentally measured and predicted ignition delay times. Eq. (3) shows the definition of the deviation factor.

$$d(T) = \left(IDT^{exp}(T) - IDT^{sim}(T)\right)/IDT^{exp}(T) \quad (3)$$

Where d is the deviation factor, IDT^{exp} is the experimentally measured ignition delay time, and IDT^{sim} is the simulated ignition delay times using the unmodified kinetic mechanism. A corrected sensitivity coefficient can be obtained by computing the sensitivity coefficient under the same conditions as the experimental measurements and by multiplying it by the deviation factor. This way, only reactions showing high sensitivity in the regions where the mechanism performs the worst show high corrected sensitivity values. Fig. 14 shows a graphical representation of the computation of corrected sensitivity values. It is important to note that the deviation can be negative, therefore, the corrected sensitivity coefficient can have an opposite sign with respect to the sensitivity coefficient. A positive corrected sensitivity coefficient means that an increase in the reaction rate decreases the deviation, while a negative corrected sensitivity coefficient means that lower errors are achieved by decreasing the reaction rate.

The sensitivity analysis was performed on the sub-mechanisms of 2,2,4,6,6-pentamethylheptane (isododecane), and 2,2,4,4,6,8,8-heptamethylnonane (isocetane). These two alkanes were selected since they showed the worst performance of the sub-mechanism. Moreover, experimental data covering both high and low temperatures were available for these two alkanes. Simulations were performed in adiabatic, homogeneous, fixed-volume batch reactors with stoichiometric mixtures of fuel/air. Initial pressure was set to 20 atm and 40 atm for isododecane and isocetane respectively, consistent with referenced experimental measurements.

Fig. 15 shows the peak corrected sensitivity coefficients for the ten reactions with the highest absolute peak sensitivity coefficient. The two alkanes show similar corrected sensitivity coefficients. Of all the highlighted reactions, only the hydrogen abstraction by HO_2 radical affects the high-temperature oxidation behavior. Higher corrected sensitivity values for low-temperature reactions are expected since the highest deviations manifest in the low-temperature regime. It is important to note that large corrected sensitivity coefficients indicate that a reaction could be the source of discrepancies only if the kinetic parameters of the reaction are inaccurate. In this regard, a rigorous uncertainty evaluation of rate-rules-derived kinetic parameters is not straightforward, and is outside the scope of this work.

However, considerations on possible sources of uncertainty can be made. The concerted elimination of HO_2 from alkyl peroxy radical is the

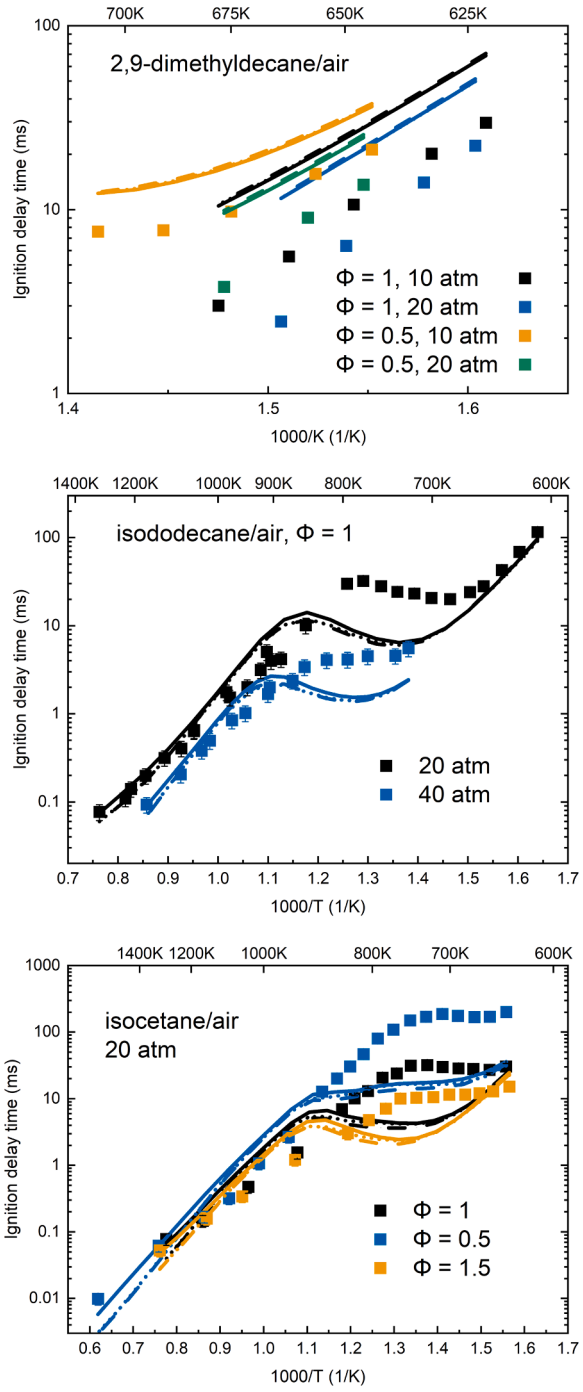

Fig. 11. Simulated (lines) and experimental [66,69,70,72,73] (symbols) ignition delay times of 2,9-dimethyldecane, 2,2,4,6,6-pentamethylheptane, and 2,2,4,4,6,8,8-heptamethylnonane. Solid lines are detailed model predictions, dashed lines are lumped model predictions based on CSTR simulations, and dotted lines are lumped model predictions based on batch reactor simulations.

reaction showing the highest corrected sensitivity coefficients, however, the adopted rate rules are computed considering all the possible substitutions of the involved carbons. Moreover, the same rate rules are shared with smaller, branched alkanes, where they perform well. Future studies could focus on assessing whether the substitution degree of the carbons neighboring the reactive sites considerably affects the reaction rate.

Similar considerations can be made on the oxygen addition to QOOH species (classes 8 and −8) and on the hydrogen abstraction by HO_2 radical (class 2). The second most important reaction class is the isomerization of alkyl peroxy radicals (classes 7 and −7). The reactions belonging to this class undergo the formation of a cyclic intermediate. The adopted rate rules do not consider the effect of substitutions on carbon atoms belonging to the formed ring, even though they could considerably affect the rate of reactions. Indeed, studies by Miyoshi [20] show that in the conversion of QOOH radicals into cyclic ethers, the formation of the cyclic intermediate is highly influenced by the presence of substitutions in the ring.

Moreover, the rate rules of reaction class −7 show no correction factor accounting for the substitution degree of the carbon bonded to the peroxy radical. The formation of cyclic ethers is another reaction class that shows large corrected sensitivity coefficients. As stated before, the rate of the reactions in this class is affected by the presence of substituted carbons in the intermediate cyclic structure. However, only the effect of tertiary and quaternary carbons in the formation of four-membered cyclic ethers is assessed in the rate rules employed. The effect of substitutions in five-membered cyclic ethers is not taken into account. The effect of tertiary and quaternary carbons in intermediate cyclic structures is also not considered in the rate rules of the reaction classes 14, −14, and 9, possibly leading to errors in the prediction of the rates for large, branched alkanes.

3.4. Lumped thermochemical properties validation

As previously stated, the computed thermochemical properties do not significantly influence the performance of the generated models. This is also valid for the lumped models since no reversible lumped reactions are defined. However, it is interesting to evaluate the effectiveness of the adopted methodology for the computation of the thermochemical properties of the lumped species. The thermodynamic properties of the lumped species define the heat release and the specific heat of the gas. Intermediate species concentrations, on the other hand, are defined by the kinetic parameters and by the thermochemical properties of the species included in the base mechanism. Therefore, temperature profiles in transient states are a good metric to evaluate the accuracy of the computed properties. Fig. 16 shows the predicted temperature profiles during the autoignition of n-hexadecane in air. The predictions of the detailed and lumped models are compared at the same progress of reaction, by normalizing the time over the ignition delay time. The temperatures simulated by the different models closely match across the entire time frame. Particularly important is the congruence of temperatures in the range between the first-stage and second-stage ignition, due to the high concentration of intermediate species.

3.5. Modeling of extremely large alkanes

The robustness and flexibility of the procedure were tested by employing it to model the oxidation of extremely large alkanes. Detailed and lumped models were generated for linear alkanes with up to 30 carbon atoms. The lumped models were generated using the concentrations in CSTR and batch reactor simulations for comparison. While there is little practical interest in modeling gas-phase oxidation of species with >20 carbon atoms, the study presented in this section tests the capabilities of the procedure to produce reasonable models outside of commonly investigated conditions. Moreover, the performance of the lumping procedure is tested against extremely large, detailed models. Experimental oxidation measurements conducted under homogeneous conditions are not available for such large alkanes, thus, validation of the proposed models cannot be performed. Therefore, this study was limited to the comparison of the reactivity of the alkanes.

Fig. 17 shows the simulated ignition delay times for different linear alkanes using the detailed model. The increase in reactivity with an increase in carbon number was predicted for all the species. The effect of chain length on the reactivity of an alkane decreases as the size of the alkane increases; this finding is consistent with those of previous studies

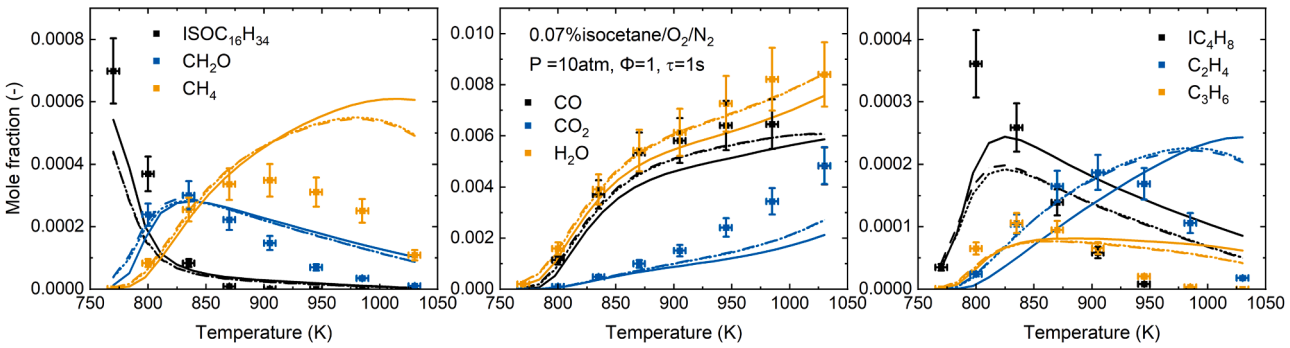

Fig. 12. Simulated (lines) and experimental [71] (symbols) species mole fractions of 2,2,4,4,6,8,8-heptamethylnonane oxidation in a jet-stirred reactor. Solid lines are detailed model predictions, dashed lines are lumped model predictions based on CSTR simulations, and dotted lines are lumped model predictions based on batch reactor simulations.

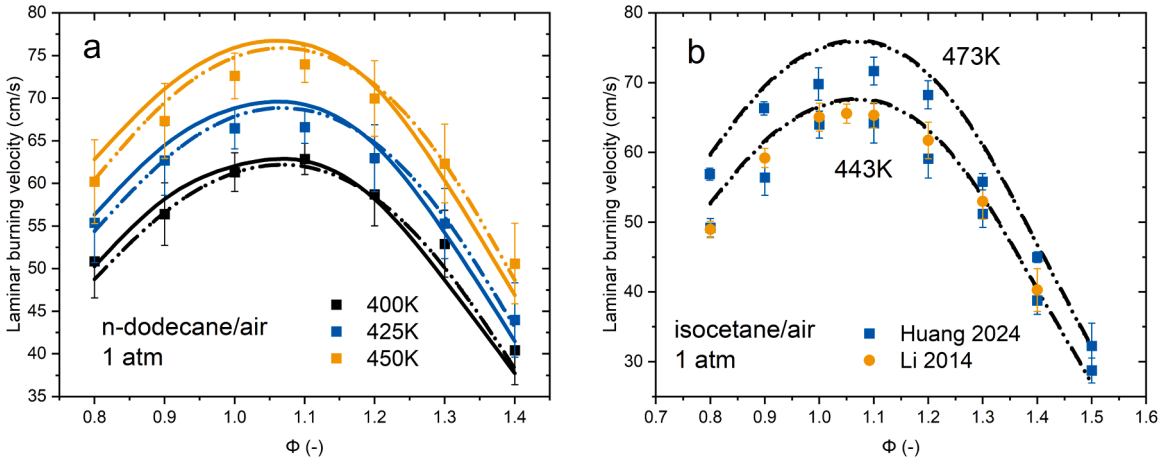

Fig. 13. Simulated (lines) and experimental [52,74,75] (symbols) laminar burning velocities for n-dodecane (a) and 2,2,4,4,6,8,8-heptamethylnonane (b). Temperatures refer to the inlet unburned gas. Solid lines are detailed model predictions, dashed lines are lumped model predictions based on CSTR simulations, and dotted lines are lumped model predictions based on batch reactor simulations.

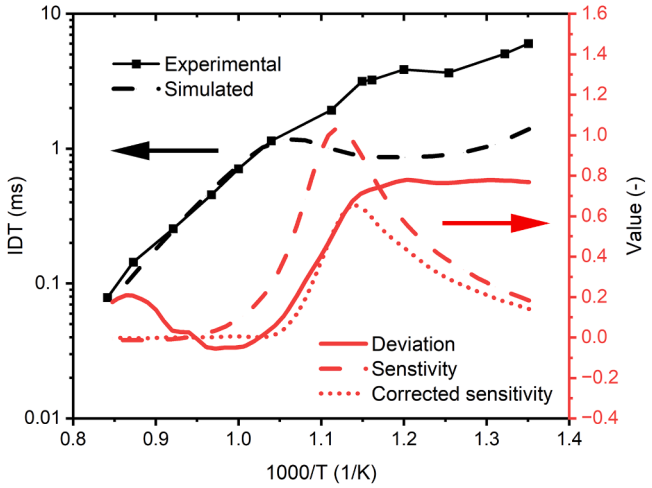

Fig. 14. Computation of the corrected sensitivity coefficient for the reaction ISOR16OO=>ISOOLE16+HO2. All simulations are performed in adiabatic, homogeneous fixed-volume batch reactors, with stoichiometric mixtures of isocetane/air at 40 atm.

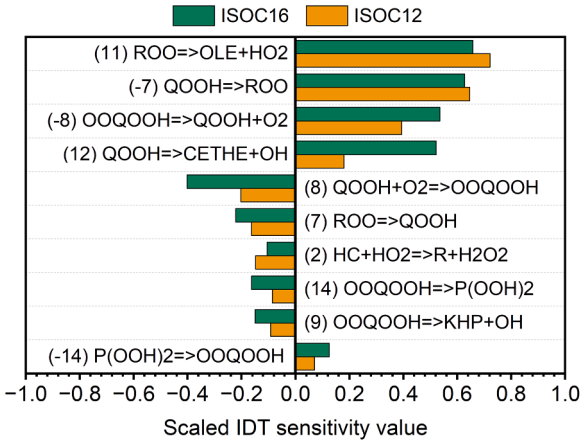

Fig. 15. Peak corrected sensitivity coefficients for the sub-mechanisms of 2,6-dimethylhexane (XC8), 2,2,4,6,6-pentamethylheptane (ISOC12), and 2,2,4,4,6,8,8-heptamethylnonane (ISOC16). The numbers in parenthesis represent the reaction class number.

[7]. Fig. 18 displays the simulated species molar fractions in jet-stirred reactors according to the detailed mechanism. The concentration profiles vary smoothly with the increase in size of the alkane. No unexpected transition is observed. Fig. 19 reports the performance of the lumping methodology for extremely large alkanes. Both lumped models closely approximate the detailed mechanism for n-triacontane (n-C30H62). The detailed and lumped mechanisms are presented in the Supplementary Materials along with more comparisons of the three

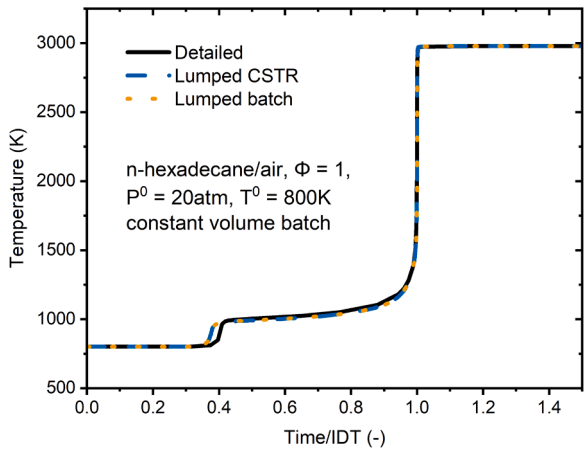

Fig. 16. Simulated temperature profiles in adiabatic, homogeneous fixed-volume batch reactors. Solid lines are detailed model predictions, dashed lines are lumped model predictions based on CSTR simulations, and dotted lines are lumped model predictions based on batch reactor simulations.

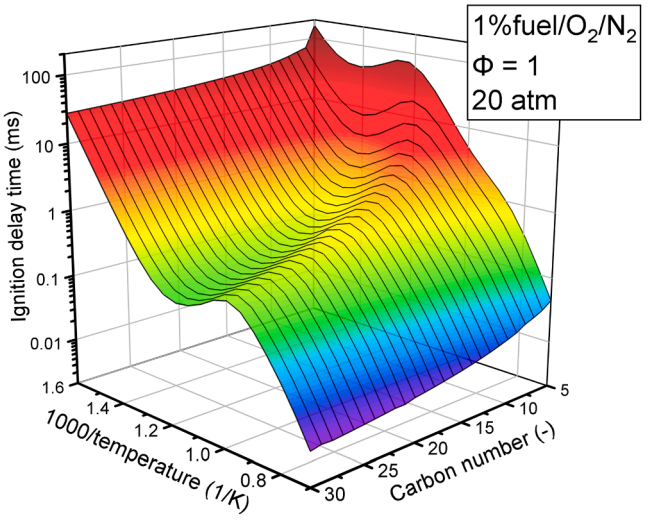

Fig. 17. Simulated ignition delay times of linear alkanes in adiabatic, homogeneous fixed-volume batch reactors. All predictions use the detailed kinetic model.

models.

3.6. Primary reference fuel modeling

The models discussed in the previous sections described pure alkane oxidation well. However, the models are too cumbersome for many applications. In most cases, the user is interested in modeling just a small set of target alkanes. The performance of the presented procedure in assisting such a task is discussed in this section.

As a case study, gasoline primary reference fuels (PRFs) were modeled. The term "gasoline PRF" refers to binary mixtures of *n*-heptane and isooctane (2,2,4-trimethylpentane) that are used to represent gasoline blends with different octane ratings. To model PRF, the software was adopted by selecting *n*-heptane and 2,2,4-trimethylpentane as the only targets. This means that the software generates the complete oxidation sub-mechanisms only for the two selected alkanes. Then, the software generates only the necessary missing reactions to close the gap between the sub-mechanisms of the two alkanes and the chosen core/base model.

Following this procedure, a detailed and two lumped models were

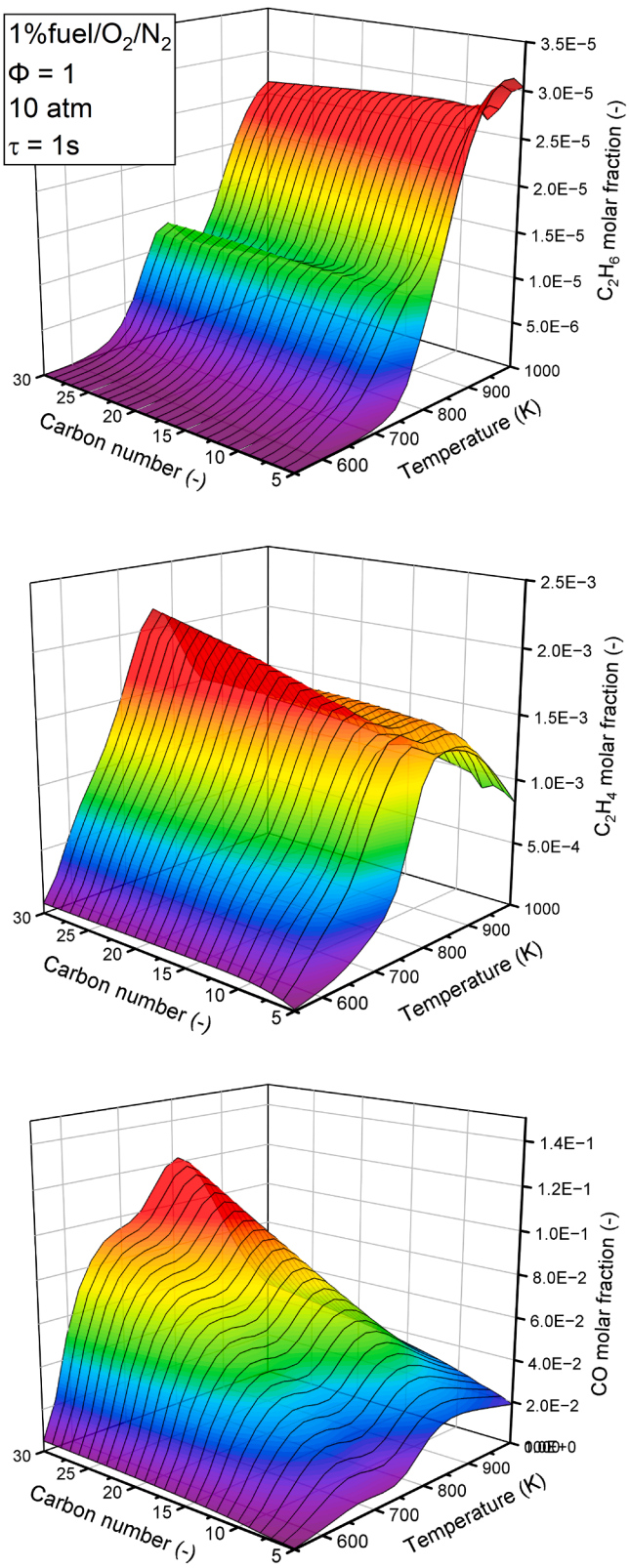

Fig. 18. Simulated species molar fraction for linear alkanes in a jet-stirred reactor. All predictions use the detailed kinetic model.

generated. The two lumped models are based on CSTR and batch reactor simulations. This approach ensures that the model size is minimized. The detailed model adds 2097 reactions and 697 species to the core/base model, while the lumped models add only 247 reactions and 102

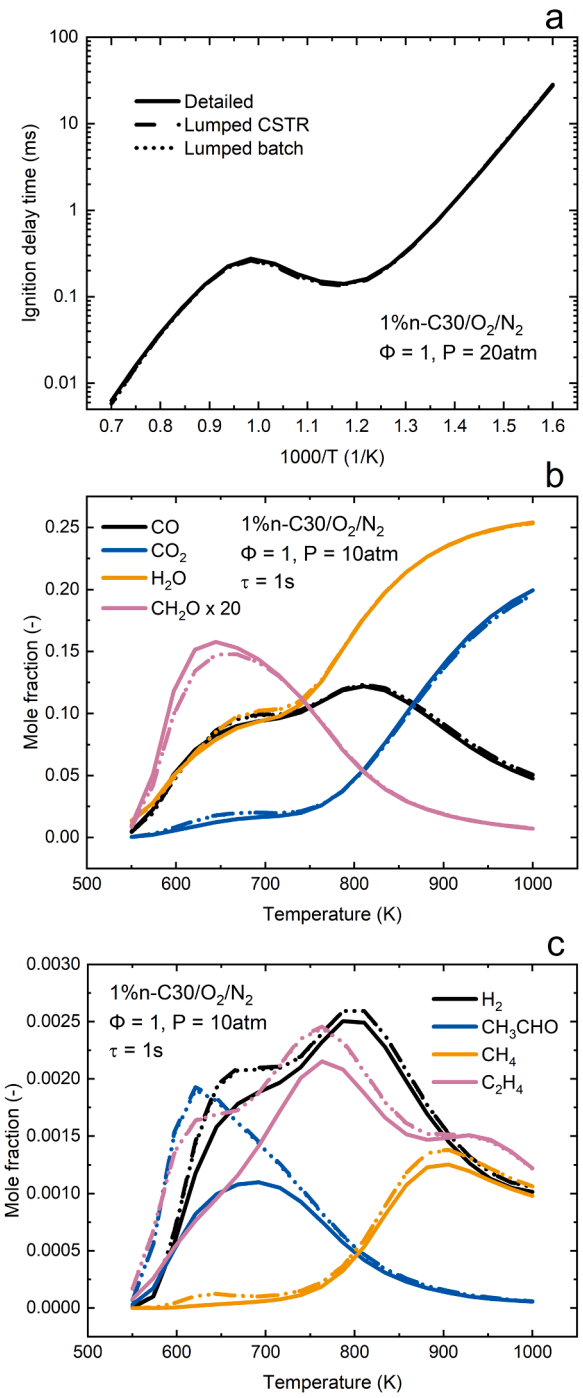

Fig. 19. Predicted ignition delay times (a) and species concentrations in jet-stirred reactors (b and c) for the oxidation of n-triacontane. Solid lines are detailed model predictions, dashed lines are lumped model predictions based on CSTR simulations, and dotted lines are lumped model predictions based on batch reactor simulations.

species. The generated models were validated against experimental measurements of ignition delay times in shock tubes [77]. The simulated ignition delay times were the simulated time from the beginning of the simulation to the time of maximum temperature gradient in volume-constrained, homogeneous, adiabatic batch simulations. The volume of the reactor was set to vary in time to represent an adiabatic compression with a pressure increase of 3 %/ms to account for the experimentally measured pressure profile.

Fig. 20 compares the simulated and measured ignition delay times

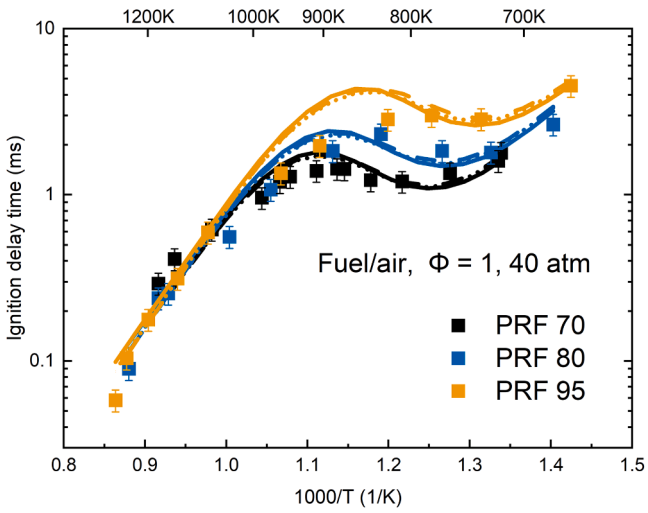

Fig. 20. Simulated (lines) and experimental [77] (symbols) ignition delay times for different gasoline primary reference fuel blends. Solid lines are detailed model predictiosn, dashed lines are lumped model predictions based on CSTR simulations, and dotted lines are lumped model predictions based on batch reactor simulations.

for three PRF blends. The number used for labeling the PRF blends refers to the volume fraction of isooctane in the liquid isooctane/*n*-heptane blend. For example, PRF 70 comprises 70 % isooctane and 30 % *n*-heptane by volume, referred to the blend in the liquid phase. The detailed and lumped models predict the reactivity of the blends. The models reproduce a decreasing trend of reactivity with an increase in isooctane concentration. The predictions of laminar burning velocities for n-heptane and isooctane were compared against experimental data [78–82] as shown in Fig. 21. Reduced versions of the models, accounting only for high-temperature chemistry, were adopted for the computation of laminar burning velocities. Mechanisms reduction and transport properties calculation were performed with the same methodology described previously. Predicted laminar burning velocities match experimental measurements for fuel-lean, stoichiometric, and moderately fuel-rich conditions. The models underpredict flame speed for a range of fuel-rich conditions. Lumped models closely approximate the detailed model under all investigated conditions. The detailed and lumped models for gasoline PRF are given in the Supplementary Materials.

4. Conclusions

This work presented a software tool for the automatic generation of compact kinetic models for the oxidation of large alkanes. An updated set of rate rules for the oxidation of alkanes with >11 carbon atoms was implemented, thereby improving the prediction of the combustion properties of large alkanes. Automatic thermochemical data prediction is included in the proposed software package, allowing a user to obtain complete combustion models. The proposed software also detects missing decomposition pathways and adds them as needed. This allows for reducing the gap between the sub-mechanisms of large alkanes and the core mechanism while reducing the reaction mechanism size.

The proposed automatic lumping procedure was effective in greatly reducing the number of species in the model. The methodology is simple and fully automatic, only requiring the user to define the target fuels. It also allows rapid generation of the kinetic models. The detailed and lumped models, comprising oxidation sub-mechanisms for 40 linear and branched alkanes in the C_6–C_{16} range, were extensively validated against experimental measurements over a broad range of conditions. The detailed model accurately represents the oxidation of linear alkanes over a wide range of temperatures, pressures, and operating conditions.

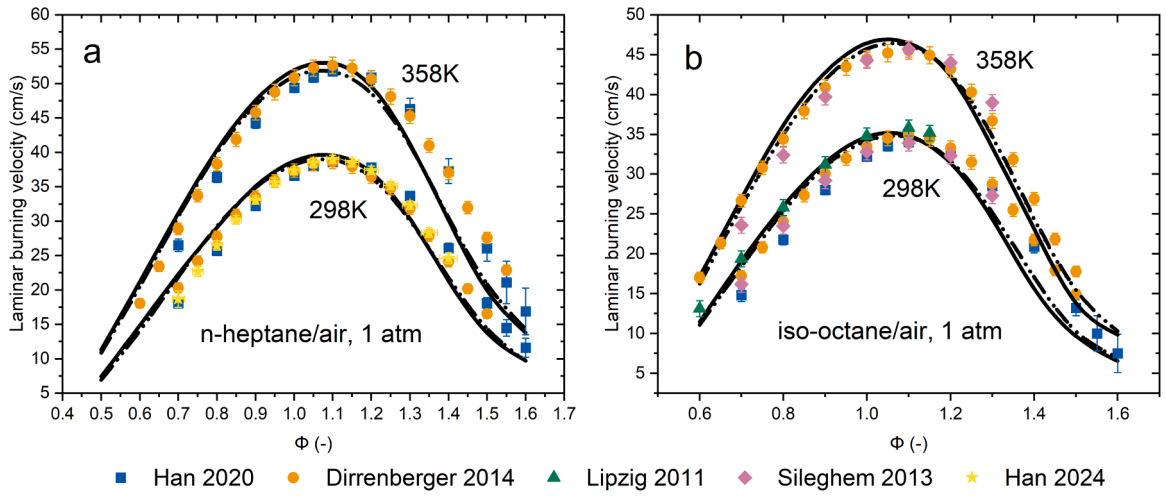

Fig. 21. Simulated (lines) and experimental [78–82] (symbols) laminar burning velocities for n-heptane (a) 2,2,4-trimethylpentane (b). Temperatures refer to the inlet unburned gas. Solid lines are detailed model predictions, dashed lines are lumped model predictions based on CSTR simulations, and dotted lines are lumped model predictions based on batch reactor simulations.

However, lower accuracy was achieved in predicting the oxidation of large alkanes in the NTC regime. The discrepancies are mainly attributed to the complexity of defining consistent rate rules applicable to large, branched alkanes. This reasoning is supported by the studies of Miyoshi [20] and Villano et al. [28], which demonstrated complex relations between the formation rates of cyclic ethers and their molecular structures.

The lumped models closely represented the detailed model under all the investigated conditions, despite the substantial reduction in the number of species involved. The two lumped models, based on CSTR or batch reactor simulations, showed almost identical behaviors, proving that the lumped models are predictive and applicable to a wider range of conditions.

The capabilities of the proposed procedure were tested. A kinetic model for extremely large normal alkanes (up to 30 carbon atoms) was generated. The obtained model predicts the expected trend of reactivity without any aberrant results. In another case study, a kinetic model for gasoline primary reference fuels was generated. In this case, the minimum set of target alkanes was specified to limit the reaction mechanism size. The model was validated against experimental measurements and showed good performance. In all the investigated cases, the lumping procedure generated compact mechanisms capable of closely representing the detailed counterpart.

Future developments of the procedure will aim to define improved, consistent rate rules for representing the low-temperature oxidation of large, branched alkanes.

CRediT authorship contribution statement

Sirio Brunialti: Writing – review & editing, Writing – original draft, Visualization, Validation, Software, Methodology, Investigation, Funding acquisition, Formal analysis, Data curation, Conceptualization. **Xiaoyuan Zhang:** Writing – review & editing, Writing – original draft, Validation, Methodology, Investigation, Formal analysis, Data curation, Conceptualization. **Qi Wang:** Writing – review & editing. **Tiziano Faravelli:** Writing – review & editing, Supervision. **S. Mani Sarathy:** Writing – review & editing, Supervision, Project administration, Funding acquisition.

Declaration of completing interest

The authors declare that they have no known competing financial interests or personal relationships that could have appeared to influence the work reported in this paper.

Acknowledgements

S. Brunialti was supported by the Al-Khwarizmi KAUST Fellowship.

Supplementary materials

Supplementary material associated with this article can be found, in the online version, at doi:10.1016/j.combustflame.2025.114355.

References

[1] D. Bothe, C. Gatzen, M. Reger, M. Lothmann, F. Duennebeil, K. Biemann, A. Liebich, M. Dittrich, S. Limberger, M. Rosental, T. Fröhlich, U. Kramer, FVV future Fuels Study IV - the transformation of mobility to the GHG-neutral post-fossil age - H1269 2021-10 EN, 2023.
[2] F.S. Zeman, D.W. Keith, Carbon neutral hydrocarbons, Philos. T R Soc. A 366 (2008) 3901–3918.
[3] C.W. Gao, J.W. Allen, W.H. Green, R.H. West, Reaction mechanism Generator: automatic construction of chemical kinetic mechanisms, Comput. Phys. Commun. 203 (2016) 212–225.
[4] V. Warth, F. Battin-Leclerc, R. Fournet, P.A. Glaude, G.M. Côme, G. Scacchi, Computer based generation of reaction mechanisms for gas-phase oxidation, Comput. Chem. 24 (2000) 541–560.
[5] E. Ranzi, A. Frassoldati, S. Granata, T. Faravelli, Wide-range kinetic modeling study of the pyrolysis, partial oxidation, and combustion of heavy n-alkanes, Ind. Eng. Chem. Res. 44 (2005) 5170–5183.
[6] C.K. Westbrook, M. Mehl, W.J. Pitz, G. Kukkadapu, S. Wagnon, K. Zhang, Multi-fuel surrogate chemical kinetic mechanisms for real world applications, Phys. Chem. Chem. Phys. 20 (2018) 10588–10606.
[7] S.M. Sarathy, C.K. Westbrook, M. Mehl, W.J. Pitz, C. Togbe, P. Dagaut, H. Wang, M. A. Oehlschlaeger, U. Niemann, K. Seshadri, P.S. Veloo, C. Ji, F.N. Egolfopoulos, T. Lu, Comprehensive chemical kinetic modeling of the oxidation of 2-methylalkanes from C to C, Combust Flame 158 (2011) 2338–2357.
[8] E. Ranzi, T. Faravelli, P. Gaffuri, A. Sogaro, Low-temperature combustion - automatic-generation of primary oxidation reactions and lumping procedures, Combust Flame 102 (1995) 179–192.
[9] S. Brunialti, X. Zhang, T. Faravelli, A. Frassoldati, S.M. Sarathy, Automatically generated detailed and lumped reaction mechanisms for low- and high-temperature oxidation of alkanes, Proc. Combust. Inst. 39 (2023) 335–344.
[10] S.P. Heneghan, S. Zabarnick, Oxidation of jet fuels and the formation of deposit, Fuel 73 (1994) 35–43.
[11] K.W. Zhang, C. Banyon, U. Burke, G. Kukkadapu, S.W. Wagnon, M. Mehl, H. J. Curran, C.K. Westbrook, W.J. Pitz, An experimental and kinetic modeling study of the oxidation of hexane isomers: developing consistent reaction rate rules for alkanes, Combust Flame 206 (2019) 123–137.
[12] M.A. Oehlschlaeger, J. Steinberg, C.K. Westbrook, W.J. Pitz, The autoignition of iso-cetane at high to moderate temperatures and elevated pressures: shock tube experiments and kinetic modeling, Combust Flame 156 (2009) 2165–2172.
[13] Z. Wang, S.M. Sarathy, Third O2 addition reactions promote the low-temperature auto-ignition of n-alkanes, Combust Flame 165 (2016) 364–372.

[14] Z. Wang, M. Ehn, M.P. Rissanen, O. Garmash, L. Quéléver, L. Xing, M. Monge-Palacios, P. Rantala, N.M. Donahue, T. Berndt, S.M. Sarathy, Efficient alkane oxidation under combustion engine and atmospheric conditions, Commun. Chem. 4 (2021) 18.

[15] Z. Wang, D.M. Popolan-Vaida, B. Chen, K. Moshammer, S.Y. Mohamed, H. Wang, S. Sioud, M.A. Raji, K. Kohse-Höinghaus, N. Hansen, P. Dagaut, S.R. Leone, S. M. Sarathy, Unraveling the structure and chemical mechanisms of highly oxygenated intermediates in oxidation of organic compounds, Pro. Natl. Acad. Sci. 114 (2017) 13102–13107.

[16] Z. Wang, L. Zhang, K. Moshammer, D.M. Popolan-Vaida, V.S.B. Shankar, A. Lucassen, C. Hemken, C.A. Taatjes, S.R. Leone, K. Kohse-Höinghaus, N. Hansen, P. Dagaut, S.M. Sarathy, Additional chain-branching pathways in the low-temperature oxidation of branched alkanes, Combust Flame 164 (2016) 386–396.

[17] E.-A. Tingas, Z. Wang, S. Mani Sarathy, H.G. Im, D.A. Goussis, Chemical kinetic insights into the ignition dynamics of n-hexane, Combust Flame 188 (2018) 28–40.

[18] Z. Wang, B. Chen, K. Moshammer, D.M. Popolan-Vaida, S. Sioud, V.S.B. Shankar, D. Vuilleumier, T. Tao, L. Ruwe, E. Bräuer, N. Hansen, P. Dagaut, K. Kohse-Höinghaus, M.A. Raji, S.M. Sarathy, n-heptane cool flame chemistry: unraveling intermediate species measured in a stirred reactor and motored engine, Combust Flame 187 (2018) 199–216.

[19] E. Ranzi, C. Cavallotti, A. Cuoci, A. Frassoldati, M. Pelucchi, T. Faravelli, New reaction classes in the kinetic modeling of low temperature oxidation of n-alkanes, Combust Flame 162 (2015) 1679–1691.

[20] A. Miyoshi, Systematic computational study on the unimolecular reactions of alkylperoxy (RO2), hydroperoxyalkyl (QOOH), and hydroperoxyalkylperoxy (O2QOOH) radicals, J. Phys. Chem. A 115 (2011) 3301–3325.

[21] K. Zhang, C. Banyon, J. Bugler, H.J. Curran, A. Rodriguez, O. Herbinet, F. Battin Leclerc, C. B'Chir, A. Karl, An updated experimental and kinetic modeling study of n-heptane oxidation, Combust. Flame 172 (2016) 116–135.

[22] M. Mehl, W.J. Pitz, M. Sjöberg, J.E. Dec, Detailed Kinetic Modeling of Low-Temperature Heat Release for PRF Fuels in an HCCI Engine, SAE Technical Paper 2009-01-1806, SAE International, 2009.

[23] L. Cai, H. Pitsch, S.Y. Mohamed, V. Raman, J. Bugler, H. Curran, S.M. Sarathy, Optimized reaction mechanism rate rules for ignition of normal alkanes, Combust Flame 173 (2016) 468–482.

[24] C.K. Westbrook, W.J. Pitz, O. Herbinet, H.J. Curran, E.J. Silke, A comprehensive detailed chemical kinetic reaction mechanism for combustion of n-alkane hydrocarbons from n-octane to n-hexadecane, Combust. Flame 156 (2008) 181–199.

[25] H.J. Curran, P. Gaffuri, W.J. Pitz, C.K. Westbrook, A comprehensive modeling study of iso-octane oxidation, Combust Flame 129 (2002) 253–280.

[26] A. Miyoshi, Molecular size dependent falloff rate constants for the recombination reactions of alkyl radicals with O2 and implications for simplified kinetics of alkylperoxy radicals, Int. J. Chem. Kinet. 44 (2012) 59–74.

[27] S. Sharma, S. Raman, W.H. Green, Intramolecular hydrogen migration in alkylperoxy and hydroperoxyalkylperoxy radicals: accurate treatment of hindered rotors, J. Phys. Chem. A. 114 (2010) 5689–5701.

[28] S.M. Villano, L.K. Huynh, H.-H. Carstensen, A.M. Dean, High-pressure rate rules for alkyl + O2 reactions. 2. The isomerization, cyclic ether formation, and β-scission reactions of hydroperoxy alkyl radicals, J. Phys. Chem. A 116 (2012) 5068–5089.

[29] S. Brunialti, X.Y. Zhang, T. Faravelli, A. Frassoldati, S.M. Sarathy, Automatically generated detailed and lumped reaction mechanisms for low- and high-temperature oxidation of alkanes, Proc. Combust. Inst. 39 (2023) 335–344.

[30] E. Ranzi, M. Dente, A. Goldaniga, G. Bozzano, T. Faravelli, Lumping procedures in detailed kinetic modeling of gasification, pyrolysis, partial oxidation and combustion of hydrocarbon mixtures, Prog. Energy Combust. Sci. 27 (2001) 99–139.

[31] H. Huang, M. Fairweather, J.F. Griffiths, A.S. Tomlin, R.B. Brad, A systematic lumping approach for the reduction of comprehensive kinetic models, Proc. Combust. Inst. 30 (2005) 1309–1316.

[32] L. Heberle, P. Pepiot, Automatic identification and lumping of high-temperature fuel decomposition pathways for chemical kinetics mechanism reduction, Proc. Combust. Inst. 38 (2021) 1053–1061.

[33] P. Pepiot-Desjardins, H. Pitsch, An automatic chemical lumping method for the reduction of large chemical kinetic mechanisms, Combust. Theory Model. 12 (2008) 1089–1108.

[34] M. Sarathy, N. Atef, A. Alfazazi, J. Badra, Y. Zhang, T. Tzanetakis, Y. Pei, Reduced gasoline surrogate (Toluene/n-Heptane/iso-Octane) chemical kinetic model for compression ignition simulations, 2018.

[35] D.G. Goodwin, K. Moffat, I. Schoegl, R.L. Speth, B.W. Weber, Cantera: an object-oriented software toolkit for chemical kinetics, thermodynamics, and transport processes, 2023.

[36] S.G. Johnson, The NLopt nonlinear-optimization package, 2007.

[37] S.W. Benson, J.H. Buss, Additivity rules for the estimation of molecular properties. Thermodynamic properties, J. Chem. Phys. 29 (1958) 546–572.

[38] ANSYS Chemkin-Pro: a Chemical Kinetics Package For Analysis of Gas-Phase Chemical Kinetics, Reaction Design, 2019.

[39] M.J. McNenly, R.A. Whitesides, D.L. Flowers, Faster solvers for large kinetic mechanisms using adaptive preconditioners, Proc. Combust. Inst. 35 (2015) 581–587.

[40] A. Cuoci, A. Frassoldati, T. Faravelli, E. Ranzi, OpenSMOKE plus plus : an object-oriented framework for the numerical modeling of reactive systems with detailed kinetic mechanisms, Comput. Phys. Commun. 192 (2015) 237–264.

[41] Y. Li, C.-W. Zhou, K.P. Somers, K. Zhang, H.J. Curran, The oxidation of 2-butene: a high pressure ignition delay, kinetic modeling study and reactivity comparison with isobutene and 1-butene, Proc. Combust. Inst. 36 (2017) 403–411.

[42] Z. Wang, O. Herbinet, Z. Cheng, B. Husson, R. Fournet, F. Qi, F. Battin-Leclerc, Experimental investigation of the low temperature oxidation of the five isomers of hexane, J. Phys. Chem. A 118 (2014) 5573–5594.

[43] O. Herbinet, B. Husson, Z. Serinyel, M. Cord, V. Warth, R. Fournet, P.A. Glaude, B. Sirjean, F. Battin-Leclerc, Z. Wang, M. Xie, Z. Cheng, F. Qi, Experimental and modeling investigation of the low-temperature oxidation of n-heptane, Combust. Flame 159 (2012) 3455–3471.

[44] H.K. Ciezki, G. Adomeit, Shock-tube investigation of self-ignition of N-heptane air mixtures under engine relevant conditions, Combust Flame 93 (1993) 421–433.

[45] B. Husson, O. Herbinet, P.A. Glaude, S.S. Ahmed, F. Battin-Leclerc, Detailed product analysis during low- and intermediate-temperature oxidation of ethylcyclohexane, The J. Phys. Chem. A 116 (2012) 5100–5111.

[46] S. Yamada, D. Shimokuri, S. Shy, T. Yatsufusa, Y. Shinji, Y.R. Chen, Y.C. Liao, T. Endo, Y. Nou, F. Saito, Y. Sakai, A. Miyoshi, Measurements and simulations of ignition delay times and laminar flame speeds of nonane isomers, Combust Flame 227 (2021) 283–295.

[47] J. Biet, M.H. Hakka, V. Warth, P.-A. Glaude, F. Battin-Leclerc, Experimental and modeling study of the low-temperature oxidation of large alkanes, Energy Fuels 22 (2008) 2258–2269.

[48] U. Pfahl, K. Fieweger, G. Adomeit, Self-ignition of diesel-relevant hydrocarbon-air mixtures under engine conditions, Twenty-Sixth Sympos. Combust. 26 (1996) 781–789. Vols 1 and 2.

[49] A. Mzé-Ahmed, K. Hadj-Ali, P. Dagaut, G. Dayma, Experimental and modeling study of the oxidation kinetics of n-undecane and n-dodecane in a jet-stirred reactor, Energy Fuels 26 (2012) 4253–4268.

[50] W. Zhang, L.-Y. Xian, K.-L. Yong, J.-N. He, C.-H. Zhang, P. Li, X.-Y. Li, A shock tube study of n-undecane/air ignition delays over a wide range of temperatures, Acta Physico-Chimica Sinica 32 (2016) 2216–2222.

[51] Y.B. Mao, M. Raza, Z.Y. Wu, J.Z. Zhu, L. Yu, S.X. Wang, L. Zhu, X.C. Lu, An experimental study of n-dodecane and the development of an improved kinetic model, Combust Flame 212 (2020) 388–402.

[52] N. Rajesh, C. Prathap, Investigation on the laminar burning velocity and flame stability of premixed n-dodecane-air mixtures at elevated pressures and temperatures, Fuel 318 (2022) 123347.

[53] A. Mzé-Ahmed, P. Dagaut, G. Dayma, P. Diévart, K. Hadj-Ali, Experimental study of the oxidation of N-tetradecane in a jet-stirred reactor (JSR) and detailed chemical kinetic modeling, Combustion Sci. Technol. 186 (2014) 594–606.

[54] H.-P.S. Shen, J. Steinberg, J. Vanderover, M.A. Oehlschlaeger, A shock tube study of the ignition of n-heptane, n-decane, n-dodecane, and n-tetradecane at elevated pressures, Energy Fuels 23 (2009) 2482–2489.

[55] M. Raza, J.Z. Zhu, W.J. Zhong, F. Yuan, Y.B. Mao, S.X. Wang, X.C. Lu, An experimental and kinetic modeling study of gas-phase autoignition of n-pentadecane at low-to-high temperatures and elevated pressures, Fuel 287 (2021) 119558.

[56] M. Assad, V. Leschevich, O. Penyazkov, K. Sevrouk, V. Tangirala, D. JD, Autoignitions of N-hexadecane and heptamethylnonane at high temperatures, nonequilibrium phenomena, Plasma, Combust. Atmosph. (2009).

[57] D.R. Haylett, D.F. Davidson, R.K. Hanson, Ignition delay times of low-vapor-pressure fuels measured using an aerosol shock tube, Combust Flame 159 (2012) 552–561.

[58] L. Yu, W. Wang, S. Wang, Y. Feng, Y. Qian, X. Lu, An experimental and modeling study of n-hexadecane autoignition under low-to-intermediate temperatures, Sci. China Technol. Sci. 63 (2020) 719–730.

[59] S.Y. Mohamed, L. Cai, F. Khaled, C. Banyon, Z. Wang, M.J. Al Rashidi, H. Pitsch, H. J. Curran, A. Farooq, S.M. Sarathy, Modeling ignition of a heptane isomer: improved thermodynamics, reaction pathways, kinetics, and rate rule optimizations for 2-methylhexane, J. Phys. Chem. A 120 (2016) 2201–2217.

[60] R. Choudhary, J.J. Girard, S. Clees, S.E. Johnson, J. Shao, D.F. Davidson, R. K. Hanson, A.A. Aradi, Measurement of time histories of stable intermediates during first stage ignition of n-heptane and its two isomers in a shock tube, Proc. Combust. Inst. 38 (2021) 957–965.

[61] Z. Wang, N. Hansen, A.W. Jasper, B. Chen, D.M. Popolan-Vaida, K.K. Yalamanchi, A. Najjar, P. Dagaut, S.M. Sarathy, Cool flame chemistry of diesel surrogate compounds: n-decane, 2-methylnonane, 2,7-dimethyloctane, and n-butylcyclohexane, Combust Flame 219 (2020) 384–392.

[62] F. Karsenty, S.M. Sarathy, C. Togbé, C.K. Westbrook, G. Dayma, P. Dagaut, M. Mehl, W.J. Pitz, Experimental and kinetic modeling study of 3-methylheptane in a jet-stirred reactor, Energy Fuels 26 (2012) 4680–4689.

[63] S.M. Sarathy, T. Javed, F. Karsenty, A. Heufer, W. Wang, S. Park, A. Elwardany, A. Farooq, C.K. Westbrook, W.J. Pitz, M.A. Oehlschlaeger, G. Dayma, H.J. Curran, P. Dagaut, A comprehensive combustion chemistry study of 2,5-dimethylhexane, Combust Flame 161 (2014) 1444–1459.

[64] T. He, D. Kim, T. Dillstrom, K. Cai, P. Zhang, C. Liu, X. He, Z. Wang, A. Violi, Oxidation of 2,6-dimethylheptane at low temperature: kinetic modeling and experimental study, Fuel 287 (2021) 119220.

[65] S. Li, S.M. Sarathy, D.F. Davidson, R.K. Hanson, C.K. Westbrook, Shock tube and modeling study of 2,7-dimethyloctane pyrolysis and oxidation, Combust Flame 162 (2015) 2296–2306.

[66] K. Min, D. Valco, A. Oldani, T. Lee, A Reactivity Study of Jet Fuel Relevant Pure Hydrocarbon Components in a Rapid Compression Machine, 6, Energy, 2017.

[67] N. Atef, G. Issayev, S.Y. Mohamed, A. Najjar, Z. Wang, J.-Y. Wang, A. Farooq, S. M. Sarathy, Chemical kinetic study of triptane (2,2,3-trimethylbutane) as an anti-knock additive, Combust Flame 210 (2019) 399–412.

[68] N. Atef, G. Kukkadapu, S.Y. Mohamed, M. Al Rashidi, C. Banyon, M. Mehl, K. A. Heufer, E.F. Nasir, A. Alfazazi, A.K. Das, C.K. Westbrook, W.J. Pitz, T.F. Lu, A. Farooq, C.J. Sun, H.J. Curran, S.M. Sarathy, A comprehensive iso-octane

combustion model with improved thermochemistry and chemical kinetics, Combust Flame 178 (2017) 111–134.
[69] Y.B. Mao, Y. Feng, Z.Y. Wu, S.X. Wang, L. Yu, M. Raza, Y. Qian, X.C. Lu, The autoignition of iso-dodecane in low to high temperature range: an experimental and modeling study, Combust Flame 210 (2019) 222–235.
[70] S.H. Won, F.M. Haas, A. Tekawade, G. Kosiba, M.A. Oehlschlaeger, S. Dooley, F. L. Dryer, Combustion characteristics of C4 iso-alkane oligomers: experimental characterization of iso-dodecane as a jet fuel surrogate component, Combust Flame 165 (2016) 137–143.
[71] P. Dagaut, K. Hadj-Ali, Chemical kinetic study of the oxidation of isocetane (2,2,4,4,6,8,8-Heptamethylnonane) in a jet-stirred reactor: experimental and modeling, Energy & Fuels 23 (2009) 2389–2395.
[72] M. Raza, J.Z. Zhu, Y.B. Mao, S.X. Wang, X.C. Lu, The autoignition of heptamethylnonane at moderate-to-high temperatures and elevated pressures: shock tube study and improved chemical kinetic model, Fuel 281 (2020) 118787.
[73] L. Yu, Y. Qiu, Y.B. Mao, S.X. Wang, C. Ruan, W.C. Tao, Y. Qian, X.C. Lu, A study on the low-to-intermediate temperature ignition delays of long chain branched paraffin: iso-cetane, Proc. Combust. Inst. 37 (2019) 631–638.
[74] L. Huang, H. Zhao, S. Huang, Y. Mao, Y. Zuo, Q. Zhu, Measurements of laminar and turbulent flame propagation of iso-octane/air and iso-cetane/air mixtures at elevated pressures and temperatures, Combust Flame 265 (2024) 113510.
[75] B. Li, H. Zhang, F.N. Egolfopoulos, Laminar flame propagation of atmospheric iso-cetane/air and decalin/air mixtures, Combust Flame 161 (2014) 154–161.
[76] M.F. Campbell, D.F. Davidson, R.K. Hanson, Scaling relation for high-temperature biodiesel surrogate ignition delay times, Fuel 164 (2016) 151–159.
[77] M. AlAbbad, T. Javed, F. Khaled, J. Badra, A. Farooq, Ignition delay time measurements of primary reference fuel blends, Combust Flame 178 (2017) 205–216.
[78] X. Han, Z. Wang, Y. He, S. Wang, Y. Liu, A.A. Konnov, Temperature dependence of the laminar burning velocity for n-heptane and iso-octane/air flames, Fuel 276 (2020) 118007.
[79] P. Dirrenberger, P.A. Glaude, R. Bounaceur, H.Le Gall, A.P. da Cruz, A.A. Konnov, F. Battin-Leclerc, Laminar burning velocity of gasolines with addition of ethanol, Fuel 115 (2014) 162–169.
[80] J.P.J. van Lipzig, E.J.K. Nilsson, L.P.H. de Goey, A.A. Konnov, Laminar burning velocities of n-heptane, iso-octane, ethanol and their binary and tertiary mixtures, Fuel 90 (2011) 2773–2781.
[81] L. Sileghem, V.A. Alekseev, J. Vancoillie, K.M. Van Geem, E.J.K. Nilsson, S. Verhelst, A.A. Konnov, Laminar burning velocity of gasoline and the gasoline surrogate components iso-octane, n-heptane and toluene, Fuel 112 (2013) 355–365.
[82] X. Han, W. Weng, Y. He, Z. Wang, A.A. Konnov, Experimental and kinetic modelling study on the laminar burning velocities of ultra-lean n-heptane flames at atmospheric pressure, Combust Flame 268 (2024) 113613.